NASA TN D-587

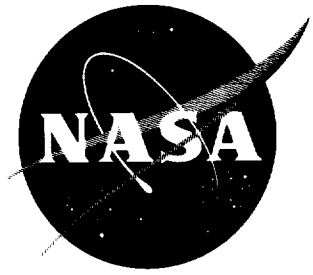

TECHNICAL NOTE

D-587

ANALYSIS OF LIQUID-HYDROGEN STORAGE PROBLEMS FOR UNMANNED NUCLEAR-POWERED MARS VEHICLES

By R. J. Brun, J. N. B. Livingood, E. G. Rosenberg, and D. W. Drier

Lewis Research Center
Cleveland, Ohio

NATIONAL AERONAUTICS AND SPACE ADMINISTRATION

WASHINGTON

January 1962

CONTENTS

E-974

NATIONAL AERONAUTICS AND SPACE ADMINISTRATION

TECHNICAL NOTE D-587

ANALYSIS OF LIQUID-HYDROGEN STORAGE PROBLEMS FOR UNMANNED NUCLEAR-POWERED MARS VEHICLES

By R. J. Brun, J. N. B. Livingood, E. G. Rosenberg, and D. W. Drier

SUMMARY

Tank geometry, tank and supporting-structure weight, meteoroid protection, size and weight of the nuclear shield, and heat inputs to the hydrogen from nuclear, on-board thermal, solar, and planetary sources are discussed for unmanned nuclear rockets probing in the vicinity of Mars and landing freight on Mars.

Cone-shaped tanks are desirable for storing hydrogen used for spiraling away from the Earth orbit, and oblate ellipsoidal tanks located inside the cone-shaped tanks are desirable for storing the hydrogen used during the second power-on phase. Meteoroid protection for a 0.92 probability of a successful mission requires a 35-percent increase in tank weight compared with tanks designed to withstand the internal pressure force only. Aluminum was chosen for this study; however, the use of beryllium and stainless steel is also discussed. A 1/8-inch coating of fibrous asbestos insulation is ample heat protection during boost.

Three vehicles with power levels of 25, 150, and 400 megawatts are considered. For the 25-megawatt vehicle, which does not employ pumps in the hydrogen circuit, no nuclear shield is required; in fact, heat must be added to the tank by a line from the reactor to obtain the boiloff rate required to cool the reactor and to maintain a constant tank pressure. For the other two vehicles, in which pumps are required, no nuclear shields are required for a selected allowable dose of 10^9 rads determined by materials and equipment limitations; however, nuclear shields are required with respect to heat input to the tank. Shields of 4 inches of LiH, weighing 150 pounds, are required to keep the heat input to the tank less than but close to that required for reactor cooling and to maintain constant tank pressure.

During coast, both the required and obtained heat inputs into the tank change with coast time. For the first few days of coast, the required heat input exceeds that obtained; therefore, heat must be added to the tank by a line from the reactor. After the first few days, more

heat than is required enters the tank. The excess vaporized hydrogen must be thrown overboard or more passed through the reactor than is required for cooling; that is, the reactor can be maintained at a temperature lower than that originally set.

INTRODUCTION

A proposal analyzed in references 1 and 2 deals with the application of nuclear energy to vehicles intended for probing in the vicinity of Mars and landing freight on Mars. Some of the basic objectives of the space vehicles and the manner of accomplishment were suggested as a result of preliminary calculations presented in reference 3. For example, reference 3 suggested placing the nuclear stage in a 300-International-nautical-mile circular orbit about the Earth by use of chemical boosters. The use of chemical boosters eliminates the problem of atmospheric contamination and permits the use of low-power reactors, on the order of 25 to 400 megawatts, for spiraling away from the Earth and acquiring escape velocity (see ref. 1).

The spiraling trajectory of the vehicle during the Earth escape phase, which is related to the reactor power, is followed by a coasting period of approximately 200 days. The only power involved during the coasting period is that used for instrument and radio operation and that required for course correction and orientation. This power will be obtained from sources other than the main nuclear reactor. The principal nuclear power is again used near Mars in order to place the vehicle in orbit around the planet or to land on the planet.

The structural and fluid-storage concepts presented herein are part of the study reported in references 1 and 2 made at the NASA Lewis Research Center. The maximum weight that can be placed in orbit with the chemical boosters establishes a maximum permissible nuclear-vehicle gross weight. For the purpose of the study, two arbitrary values of 33,000 and 81,000 pounds (15,000 and 36,700 kg) were assumed as nuclear-stage weights. The objective of the overall study, then, was further narrowed to a determination of the magnitude in payload that can be expected with nuclear space vehicles of 33,000- and 81,000-pound gross weight.

Three vehicles (1, 2, and 3 herein) are involved in the overall study. Vehicles 1 and 2 are both limited to a gross weight of 33,000 pounds, but with power levels of 25 and 150 megawatts, respectively.

Vehicle 3 is based on a gross weight of 81,000 pounds and a power level of 400 megawatts. Vehicle 1 has a coast time of 200 days; vehicles 2 and 3 have coast times of 230 days. The analysis leading to the choice of power levels is discussed in reference 1. This reference also discusses the trip time and empty weight available in a Mars orbit for unmanned missions to Mars. Reference 1, a parametric study to determine suitable reactor powers, assumes tank weight to be a percentage of the hydrogen weight. Reference 2 presents detailed designs of the vehicles in order to estimate payloads; tank weights used in reference 2 are those determined herein.

The present report discusses tank geometry, weight of tank and supporting structure, penalties for protection of the tanks from meteoroid damage, and sizes and weights of shields to protect the tank from excessive heat inputs from nuclear, thermal, and solar sources. Procedures for calculating neutron and gamma fluxes outside the nuclear shield, necessary for determining the nuclear heating rates, are presented in appendix D by John M. Smith. Areas requiring further study and experimental data are also mentioned.

VEHICLE GEOMETRY

Factors Affecting Vehicle Shape

Structural weight is an important factor governing the geometric shape of a space vehicle. In the nuclear-powered space vehicle this factor is strongly compromised with a shape factor governing the amount of nuclear radiation permitted to enter the propellant tank from the reactor. In a nuclear spacecraft using liquid hydrogen for the propellant, the total energy absorbed by the liquid before it passes through the reactor must be limited. Other sources of heat input to the tank are thermal radiation from the payload and from the control compartment, heat conduction through struts and other structural supports, Sun and Earth radiation, and aerodynamic heating while passing through the Earth's atmosphere. The rate of energy absorption by the hydrogen in the tank from these sources is negligible compared with the rate of energy absorption from nuclear radiation when the reactor is operating at design power; however, the rate of energy absorption from solar flux becomes important when integrated over the long coasting period unless parasols (thermal reflective shields) and proper vehicle orientation with respect to the Sun are provided.

The physical size of the booster and the stresses imposed on the structure during the boosting period are also large factors influencing the shape of the space vehicle. The diameter of the chemical booster influences the maximum diameter of the spacecraft. The large bending moments and the accelerating forces during the boost phase influence the design of all the structures, including the structures supporting the tank, payload, and nuclear stage on the chemical booster.

Tank Shape

It was recognized early during the conceptual design studies (ref. 3) that the tank would contribute a considerable portion of the structural weight. Therefore, the first approach was to study a spherical tank. When other factors such as nuclear radiation and accelerating and bending forces during boost period were taken into consideration, the use of one spherical tank appeared less desirable than during the early studies. Weight studies on three design concepts were made for vehicles with 25-, 150-, and 400-megawatt power levels.

Included angle. - The 10° angle (figs. 1 to 3) is common to all three tank concepts and for all three vehicles. The 10° was set by the diameter of the hydrogen tank, the nuclear radiation energy permissible into the hydrogen tank, and the weight of the shielding material placed between the tank and the reactor. The maximum diameter allowable for the nuclear stage is governed by the size of the booster rocket. It was assumed that vehicles 1 and 2 can be set on boosters with diameters of about 20 feet. Vehicle 3 was assumed compatible with the booster if its diameter does not exceed 30 feet.

The amount of nuclear radiation that enters the hydrogen tank is a function of the solid angle through which the radiation travels, regardless of the distance between the reactor and the tank. Preliminary calculations were made of total radiation resulting from the consideration of plane half-angles of 5°, 10°, and 15°. (These, when rotated about an extension of the reactor centerline, produce the radiation solid angle.) A small angle is desirable with respect to reducing the radiation energy entering the tank. As the angle is decreased, the length of the tank of a given volume is increased; consequently, the length of the entire last stage is increased, thus imposing larger bending moments in the structure, which are especially serious during the chemical-boost period. The value of 10° is a compromise resulting from the maximum diameter limited by the assumed size of the chemical booster, with proper consideration for weight of shielding and for vehicle structure.

Tank volume. - From the trajectory calculations for a specified vehicle and mission, the weights of hydrogen used for thrust production during the power-on phase from Earth orbit to coast and the power-on phase from coast to Mars are determined. The sum of these two hydrogen weights is increased by 5 percent to allow for such factors as boiloff while the vehicle is located on the launching pad and while it is boosted through the Earth's atmosphere, for filling the lines with hydrogen, and so forth. The hydrogen stored during coast includes that required for the second power-on phase plus that boiled off during coast; this boiloff will be discussed later, when shadow shields (parasols) are considered on the payload end of the tank. The volumes corresponding to the hydrogen weights are increased 5 percent to allow for ullage.

Two-spherical-tank concept. - One of the three concepts studied consists of a spherical tank immersed in the liquid hydrogen of another spherical tank (fig. 1). The hydrogen used to propel the nuclear stage from the 300-International-nautical-mile orbit to escape velocity is stored in the outer tank. The hydrogen that must be carried for either 200 or 230 days (see ref. 1) before use near Mars is stored in the inner tank. During the coasting period the outer tank provides some protection against meteoroids. (Meteoroid protection is discussed in a later section.) Also, by confining the hydrogen stored during the long coasting period in as small a space as possible, the probability of tank puncture by meteoroids is reduced. It is also felt that unknown problems of restarting after long periods of coasting at zero-gravity conditions will be reduced if the propellant is confined in a tank of small ullage.

The structure connecting the tank to the reactor is composed of stringers and x-braces acting in compression. In order to minimize the compressive and bending loads on the connecting structure during the boost period, the nuclear stage is mounted on the booster rocket with the reactor in the nose end. The reason for placing the reactor ahead of the propellants during the operation of the chemical booster is that the reactor weighs about 4000 pounds (1800 kg) as compared with over four times that amount for the propellant and tanks. Thus, the lesser mass is supported by the connecting structure during the period of largest accelerations and bending loads. The orientation of the complete nuclear stage must be reversed by 180° after it is placed in orbit and before the thrust is applied.

The dimensions and weights will be discussed in a subsequent section when the tank concepts are compared.

Multiple-spherical-tank concept. - Another concept of geometry that was analyzed for weight and performance feasibility is a group of spherical tanks arranged as shown in figure 2. The tanks are supported by a pressurized skin covering. During the boost period the tanks are supported by the pressure force of the gas contained by the shell. As with the two-sphere concept, the reactor is in the nose of the vehicle during boost period.

In this concept tanks marked A carry hydrogen for spiraling away from the Earth. Tanks B store hydrogen for either 200 or 230 days during the coasting period. The long-period storage tanks must be provided with meteoroid protection, which is considered in the weight analysis.

Cone-tank concept. - The third arrangement considered is shown in figure 3. The evolutionary change from the concept of figure 1 to that of figure 3 is to reduce the overall length of the vehicle by moving the center of mass of the liquid hydrogen closer to the reactor, while maintaining the half included angle at 10°. A change in the location of the

center of mass does not change the total nuclear radiation absorbed by the liquid hydrogen if the included angle and shielding are not changed. The reduction in length of the structure connecting the tanks with the reactor results in lower values of bending moments and a simplified structure, with a consequent decrease in structural weight.

The tank concept of figure 3 is a cone shape with an oblate ellipsoid at the large end and a hemisphere at the small end. The oblate tank at the large end of the cone stores liquid hydrogen during the long coasting period. The liquid hydrogen used for spiraling away from the Earth is stored in the large conical tank.

The choice of an ellipsoidal as compared with a spherical shape for the large end is based on the following reasoning: For an ellipsoid with a ratio of major to minor axis of 2, as is the case with the design shown in figure 3, the surface area of the ellipsoid is 9.5 percent larger than the surface area of a sphere of equal volume. However, when part of the inner ellipsoidal tank wall is combined with the wall of the outer tank, there results a 16-percent reduction in total area as compared with the case of a spherical end on the large tank and a smaller inner sphere. The resulting reduction in total surface area results in a decreased weight penalty when meteoroid protection is an important factor, because the wall thicknesses are no longer established by stress requirements. Furthermore, the analysis showed that the weight of the supporting structure for an inner sphere together with the complication in the conical tank wall necessary for tying the supporting structure compensated for any weight savings even when the design was based on stress requirements only.

Comparison of the three concepts. - The three tankage arrangements for each vehicle were compared under the same conditions regarding acceleration and bending loads during the boost period.

The largest structural loads are imposed during the boost period. Aluminum was assumed as the material for all cases. The relative weight comparison is valid regardless of the material used. All the tanks were designed to support an internal pressure of 50 pounds per square inch absolute. The tank pressure was established by the reactor requirements for vehicle 1. In vehicles 2 and 3 the vapor pressure of the top layer of hydrogen after stratification during the boost phase and orbiting phase before thrust generation was estimated to be somewhat less than 50 pounds per square inch absolute. The 50 pounds per square inch absolute, which is also gage pressure at the orbital altitude, is adequate for structural stability during the boost phase and the 180° reorientation during the orbital phase.

The essential values for comparison among the three concepts are given in table I. The conical tank has the advantages of compactness

and less weight than the other two concepts. For example, for vehicle 2 the conical tank concept, including the structure connecting the tank to the reactor, is 17 feet shorter than the cluster of spheres; and for vehicle 3 the conical concept is 18 feet shorter. Although the conical tank is heavier than a spherical tank designed for equal volume and internal pressure, the combination of tank plus supporting and connecting structure results in less weight for the conical concept than for either the two-sphere or cluster-of-spheres concepts. Because the conical shape concept resulted in the lowest weight, it is chosen for the vehicle analyses discussed in the remainder of this report.

Interstage Section

The weight of the transition section between the last chemical stage of the booster and the nuclear stage was calculated on the basis of two design principles. Each design assumed that this interstage section is discarded with the last stage of the chemical booster. One weight calculation was based on a pressure-stabilized-skin type of construction. For this construction the nuclear stage is supported by a pressure force of 20 pounds per square inch gage contained in the transition section. The other weight calculation for the interstage section is based on a stringers-and-skin design to support the loads in compression. A sketch of this section is shown in figure 4. The weights for both designs are given in table II. The values in the table apply to stainless steel, which is the recommended material that will withstand the aerodynamic temperatures encountered during the boosting period.

The weight differences, although different by a factor of 2, affect the gross weight of the nuclear stage by a small percentage and affect the final payload to Mars by considerably less than many other factors of uncertainty. Since the nonpressurized design does not depend on pressure-tight joints and requires a less complicated procedure for ground handling, the nonpressurized design is considered to be more reliable and advantageous in the overall project.

PROTECTION FROM METEOROIDS

Symbols are defined in appendix A, and the procedure for calculating the depth of meteoroid penetration as a function of an assumed probability of suffering a given penetration during a given time period in space is presented in appendix B. The craters assumed formed by the meteoroids are illustrated in figure 5.

Results of Calculations for Meteoroid Protection

Outer cone-shaped tank. - The first structure examined for meteoroid protection is the outer tank, which is designed to contain the liquid hydrogen used during the spiraling period when escape velocity is attained. This time period (including time in orbit for orientation, warmup, etc.) is 4 hours, 32 minutes, and 46 minutes for vehicles 1, 2, and 3, respectively. The tank areas exposed to possible meteoroid damage during these time periods are 1600, 1295, and 2620 square feet for the respective vehicles. The aluminum tank thickness varies from 0.034 inch at the small diameter to 0.085 inch at the large end for vehicle 2, and from 0.034 to 0.116 inch for vehicle 3 (fig. 3), in order to withstand the pressure force with a minimum overall tank weight. The use of stainless steel and beryllium is discussed later.

The curves of figure 6 give the probability of penetration as a function of the wall thickness for the three vehicles studied. The wall thicknesses for the conical tanks vary from the small-diameter end to the large end, as tabulated in figure 3. However, the probability of penetration shown in figure 6 assumes a constant wall thickness, so that an average wall thickness should be considered in the use of figure 6. The probability of penetration is less than indicated by the line showing the minimum wall thickness required to withstand the pressure force (common to all three vehicles). The results of the calculations (fig. 6) indicate that no weight penalty is necessary for a probability of penetration of less than 0.05 (at least a 0.95 probability of success) during the spiraling period for all the vehicles studied.

Inner tank. - The oblate tank at the large end of the outer conical tank stores liquid hydrogen during the long coasting period for use in the vicinity of Mars. The minimum wall thickness for the inner tank was also designed for a pressure of 50 pounds per square inch absolute. The protection offered by the outer tank, the payload, and the parasols was taken into account in calculating the inner-tank wall thickness. The same mechanism of penetration was assumed for the payload as for the tank. In order to incapacitate the vehicle by a penetration into the inner tank, the meteoroid was assumed to have melted a crater as shown in figure 5(b) through the outer-tank wall and proceeded with enough residual kinetic energy to melt a crater into the inner-tank wall deep enough to cause leakage. The payload capsule was assumed to give adequate protection to the inner tank from meteoroids approaching head on.

The results of the calculations are shown in figure 7 for aluminum tanks. As with figure 6, the curves give the probability of penetration as a function of the tank wall thickness. The coasting period is 200, 230, and 230 days for vehicles 1, 2, and 3, respectively. The inner-tank wall thickness required to support the working pressure is 0.11, 0.10, and 0.14 inch for vehicles 1, 2, and 3, respectively. The inner-wall thickness required for the pressure design specification (50 lb/sq in. abs), together with the outer-tank wall and payload, offers approximately a 0.50 probability of success.

For a 0.05 probability of penetration (0.95 probability of success), the inner-tank wall thicknesses of the three vehicles must be increased to 0.27 inch for vehicles 1 and 2 and to 0.37 inch for vehicle 3. The attendant combined weights of the outer and inner tanks are given in figure 8. The tankage weight to withstand the working pressure force alone is 2675, 2000, and 5200 pounds (1210, 910, and 2360 kg) for vehicles 1, 2, and 3, respectively; whereas, the weight is increased to 3400, 2700, and 7140 pounds (1540, 1225, and 3240 kg) for the respective vehicles for about a 0.92 probability of success. The tank weight is increased by 27, 35, and 37 percent, respectively, for the three vehicles. As can be seen from the curves of figure 8, the penalty increases rapidly above about 80-percent probability of success.

Effect of Doubling Number of Meteoroid Strikes

As noted in appendix B, the calculations for the curves of figures 6 to 8 were made on the basis of one-half of the number of strikes per 1000 square feet of surface area given in table III. The reasoning is that the strikes given in the table include both brittle and nonbrittle material. As is explained in appendix B, the composition of the meteoroids is an unknown that is quite controversial. Some writers on the subject hold that the brittle material will cause no damage; therefore, the number of strikes of nonbrittle material was arbitrarily reduced by one-half for the calculations of figures 6 to 8. In view of the arbitrariness of the reduction, weight calculations were made with the number of strikes given in table III assumed to be all made by nonbrittle material. These calculations were made for a 0.92 probability of success. The following tabulation gives the effect on weight and the increase in weight when the number of strikes is doubled:

Vehicle	1	2	3
Weight of tanks, lb (kg), with number of strikes given in table III	4016 (1820)	3220 (1460)	8470 (3840)
Weight of tanks, lb (kg), with one-half the strikes given in table III	3400 (1540)	2700 (1225)	7140 (3240)
Percentage increase in weight	18	19	19

Choice of Materials

The structural-weight data presented thus far in the report are based on aluminum 2014-T6 as the tank material. A study was made to compare aluminum with beryllium and stainless steel. The results of this study are shown in figure 9. The crosshatched portion of the bars is the weight penalty required for a probability of 0.92 of success in

withstanding meteoroid hits. The plain portion of the bars is the tank weight designed for a working pressure of 50 pounds per square inch absolute.

When protection from meteoroid penetration is not a factor, the use of aluminum results in the least weight. Beryllium offers the greatest resistance to meteoroid penetration per unit weight based on the mechanism for penetration set up in appendix B. The following properties of beryllium are advantageous over either aluminum or steel in protecting against meteoroid penetration: (1) high specific heat, (2) high melting point, and (3) high heat of fusion. The important properties of the three materials are compared in the following table:

	Aluminum	Beryllium	Stainless steel
Melting point, ^{o}F (^{o}C)	1220 (660)	2340 (1280)	2800 (1540)
Specific heat, Btu/(lb)(^{o}R)	0.215	0.46	0.108
Heat of fusion, Btu/lb	170	470	117
Specific weight, lb/cu in.	0.0975	0.0665	0.283
Ultimate strength, psi	93,000	75,000	150,000
Design stress, psi	60,000	50,000	100,000

Although the specific heat varies with temperature, the value given for comparison in the table is approximately midway between the ambient conditions in space and the melting point. The brittleness, cost, and poor fabrication properties are the principal disadvantages of beryllium, and at the time of this writing the feasibility of beryllium for tank fabrication is unknown. Metallurgical improvements may remove the difficulties, as well as improve the ratio of yield strength per unit weight as compared with aluminum. Because the properties of aluminum, especially at low temperatures, are better known than those of beryllium, aluminum was chosen for this analytical study.

NUCLEAR SHIELD

Selection of Allowable Dose

A schematic sketch of the nuclear stage is shown in figure 10. Since only unmanned missions are considered here, the allowable dose is set by material limitations. From reference 4 (table 10.1, p. 451), a value of 10^{18} neutrons and gammas per square centimeter was selected as the allowable dose. This dose, according to reference 4 (p. 18), is roughly equivalent to 10^{9} rads.

Determination of Nuclear-Shield Thicknesses and Weight

The nuclear shield must be designed for the condition of full reactor power, because nuclear heating is the dominating form of heat input into the tank when the reactor is operating. Of the two distinct power-on times required for the missions considered, the first (time to escape from Earth orbit) greatly exceeds the second (time to orbit or land on Mars). Hence, the shield is designed on a first-power-on basis.

Criterion for choice of nuclear shield. - Figure 11 shows a plot of dose rate per unit power against gamma-shield thickness with neutron-shield thickness and heat rate per unit shield area per unit power as parameters. The no-shield value of D/P_R of 0.0038×10^9 rads per hour per megawatt is shown on the figure. If this value is multiplied by the product of reactor power and first-power-on times for each vehicle (see table IV for the respective values), doses less than the allowable 10^9 rads are obtained, and hence no shields are required for protection from nuclear radiation. However, preliminary calculations showed that nuclear shields are required for vehicles 2 and 3 in order to avoid excessive hydrogen boiloff.

Nuclear-shield thicknesses and weights and corresponding doses obtained. - The nuclear-shield thicknesses required with respect to tank heat input for vehicles 2 and 3 were determined by the method discussed in appendix C. After some trial calculations, results were obtained that yielded values of Q slightly less than Q_{req} (see table IV). The heat rates required to cool the reactor and to maintain a constant tank pressure were calculated by the procedure discussed in appendix C. These were found to be 240.7, 121, and 324 Btu per second for vehicles 1, 2, and 3, respectively. The shields for vehicles 2 and 3 were found to consist of 4 inches of LiH and no iron. The weights of these shields, obtainable from figure 12, were 150 pounds each.

From figure 11, values of D/P_R for vehicles 1, 2, and 3 can now be obtained; these values are 0.0038×10^9, 0.001×10^9, and 0.001×10^9 rads per hour per megawatt. Multiplication of these values by reactor power and first-power-on times (see table IV) yielded obtained doses of approximately 0.329×10^9, 0.061×10^9, and 0.147×10^9 rads for vehicles 1, 2, and 3, respectively. For vehicle 1, even with no shield, heat must be added to the tank by a line from the reactor in order to obtain Q_{req}.

DETERMINATION OF TOTAL HEAT INPUT TO HYDROGEN

Boost Phase

Calculations were made to determine the heat input to the hydrogen tank during the boost period through the Earth's atmosphere. The calculations were made for 0, 1/8, and 1/4 inch of fibrous asbestos insulation.

The specific weight of the insulation is assumed to be 20 pounds per cubic foot. The weight of cement and/or clips for fastening and the covering for protection against aerodynamic loads and sealant against air condensate is assumed to be 0.03 pound per square foot. A value of $k = 0.0287 \times 10^{-4} + 0.02315 \times 10^{-7} T_{mean}$ (Btu/(sq ft)(sec)($^{\circ}$R/ft)) was used for the coefficient of heat transfer through the insulation and protectors. The value of k varied with the mean temperature T_{mean} between the outside and inside surfaces of the insulation.

The values of Mach number and altitude required to perform the calculations are given in table V. These values are typical for boosters of the size required to fulfill the objectives of this mission. The calculations for the heat input were made according to the method described in reference 5. The method recognizes that film boiling might occur at the inner wall, and the heat input is calculated accordingly.

For this evaluation, the heat into the tank below the liquid level is divided into that part which evaporates liquid in contact with the walls and that which raises the liquid bulk temperature. The proportioning ratio is not easily determined because of the many unknowns, such as convection currents, sloshing, and amount of temperature stratification. Two limiting calculations were made. For the bulk temperature-rise calculations, all the heat input was assumed to produce bulk temperature rise. For the hydrogen-vaporized calculations, all the heat input was assumed to produce vapor at the walls. During the boosting period the values of hydrogen evaporated and the bulk temperature rise will both be lower than shown in the following table:

Vehicle	Insulation thickness, in. (cm)	Bulk temp. rise, $^{\circ}$R	Hydrogen vaporized, lb (kg)	Weight of insulation, lb (kg)	Weight of fastenings and protective covering, lb (kg)
1	0	10.8	2620 (1188)	-----	-----
	1/8(0.3175)	.8	192 (87)	370 (168)	53(24.0)
	1/4(0.635)	.4	108 (49)	-----	-----
2	0	11.0	2100 (953)	-----	-----
	1/8(0.3175)	.8	154 (70)	300 (136)	43(19.5)
	1/4(0.635)	.5	87 (39)	-----	-----
3	0	9.0	4540 (2059)	-----	-----
	1/8(0.3175)	.7	330 (150)	580 (263)	84(38.1)
	1/4(0.635)	.4	187 (85)	-----	-----

The evaporative loss and the temperature rise with zero insulation are intolerable; however, a 1/8-inch layer of insulation appears to produce desirable results. For vehicle 2 the weight for insulating the vehicle is 343 pounds (155 kg), as compared with a possible loss of about 2100 pounds of hydrogen if no insulation were applied. Also, for this same vehicle the maximum possible temperature rise is reduced from 11° to 0.8° with 1/8 inch of insulation.

First Power-On Phase

Heat enters the hydrogen tank from both nuclear and thermal sources. During power-on, the majority of the heat input into the hydrogen comes from the nuclear radiation. Thermal heating results from (1) conduction through the conical structure from reactor to tank, (2) thermal radiation from control compartment, (3) conduction through struts from payload, (4) thermal radiation from payload, and (5) Sun-Earth radiation. Each of these heat inputs into the hydrogen is discussed in the following paragraphs.

Nuclear heat rate. - With the thicknesses of the nuclear shields already determined, the neutron and gammas fluxes, φ_N and φ_γ, can be calculated at the exterior face of the nuclear shields by the method discussed in appendix D. Application of equation (C5) then gives the nuclear heating rates of 55.2, 114, and 304 Btu per second for vehicles 1, 2, and 3, respectively. The cross-sectional areas used in equation (C5) are listed in table IV.

Conduction through conical structure from reactor to tank. - A stainless-steel conical structure 0.020 inch thick, shown in figure 10, was used to connect the reactor to the tank. A value of 1000° R for the cold end of the reactor was assumed. The hydrogen in the tank was assumed to be at 45° R, the thermal conductivity of stainless steel was taken as 5.8 Btu/(hr)(ft)(°R), and the area at the reactor end of the cone was used. The heat inputs by conduction through the conical structure were determined by use of the standard conduction equation (eq. (C9)) and found to be of the order of 0.003 Btu per second, which is negligible compared with the nuclear heating rate.

Thermal radiation from control compartment. - The thermal radiation from the control compartment to the hydrogen was calculated for each vehicle by use of equation (C9). The control compartment was assumed to be maintained at 520° R (room temperature), and the hydrogen was assumed to be maintained at 45° R in the tank. A 1-inch-thick insulation at the control-compartment end of the tank was assumed, and the insulation had an assumed thermal conductivity k_I of 0.11 (Btu)(in.)/(hr)(ft^2)(°R). The radiation form factors were obtained by use of equation (C8); these were calculated to be 0.355, 0.365, and 0.365 for vehicles 1, 2, and 3,

respectively. Values of $\alpha = 0.1$, $\epsilon = 0.1$, and $\sigma = 0.1713 \times 10^{-8}$ Btu/(hr)$(ft^2)(^oR^4)$ were used. The resulting values of heat input were about 0.002 Btu per second for each vehicle. These values are also negligible compared with the nuclear heating.

Conduction through struts from payload. - Some kind of supporting structure is necessary between the payload and tank. Reference 6 discusses the use of laminated supports or struts consisting of many layers of thin stainless steel or other relatively poor-conducting metals. Such laminated supports, however, are used only for compressive loads, according to reference 6.

Eight 1-inch-diameter laminated struts were originally considered; one is shown in figure 10. A payload to tank separation distance of 1 foot was assumed, and a payload temperature-regulating device was assumed to maintain a payload temperature of 520^o R. The resulting heat-input rates into the tank (0.000335 Btu/sec) proved negligible for each vehicle compared with the nuclear heating rates. Subsequent calculations made for the same size solid struts, useful for both compressive and tensile loads, also yielded negligible heat-rate inputs into the tank.

Thermal radiation from payload. - During power-on, the nuclear heating is by far the predominant form of heat input into the hydrogen. On the other hand, during coast, nuclear afterheat plays a subordinate role, and parasols (shadow shields) on the tank at the payload end are required to keep thermal radiation from the payload at a reasonable level (see fig. 10). A discussion of the optimum number and spacing of shields required will be given under the coast-phase heat-input study. Suffice it to state here that, after the numbers of shields were determined, the thermal radiation from the payload for power-on turned out to be about 0.0008 Btu per second for each vehicle, and once again this input is negligible compared with the nuclear heating.

Sun-Earth radiation. - Heat input into the hydrogen due to Sun-Earth radiation is discussed in reference 7. Figure 13 shows the various heat inputs into a cubical tank due to Sun-Earth radiation. It was assumed that the vehicle was on the Sun-Earth axis. For each vehicle considered, the cubical tank is sized so that its volume will equal that of the actual conical tank, 5325, 4045, and 9983 cubic feet for vehicles 1, 2, and 3, respectively. The sides of the equivalent cubical tanks were found to be 305, 255, and 470 square feet, respectively. The use of cubical tanks simplified the calculation of the various radiation form factors F_H and F_V. These form factors depend upon the radius of the Earth and the altitude of the vehicle above the Earth (see ref. 7). Since these form factors decrease as altitude increases, a precise calculation of the effect of Earth radiation would require integration along the escape trajectory. In addition, the inclination of the escape orbit, the time of day of initiating the escape orbit, the

season of the year, the cloud cover of the Earth, and thrust-to-weight ratio of the vehicle all would have an effect on the propellant heating resulting from Earth radiation during the escape trajectory. For the three vehicles considered herein, it was conservatively assumed that the heating effect of the Earth during escape could be calculated by using constant form factors evaluated at an altitude of 125 percent of the altitude at the beginning of the escape trajectory.

E-974

The same thickness and thermal conductivity of the insulation as used previously were employed here. A tank coating of Al_2O_3 was assumed, with corresponding values of absorptivity $\alpha = 0.168$ and emissivity $\epsilon = 0.77$.

Sun-Earth radiation for vehicles 1, 2, and 3 was calculated according to appendix C, and the resulting values are listed in table VI. Table VI summarizes the heat input to the hydrogen for the first power-on phase. From the table it can be seen that, for vehicle 1, which does not use pumps, a considerable amount of additional heat must be added by use of a line from the reactor in order to obtain the hydrogen vapor rate required to cool the reactor and to maintain the tank at constant pressure. For vehicles 2 and 3, which use pumps, the heat input is almost equal to that required, and only a small amount of additional heat must be added from the reactor.

Second Power-On Phase

For the second power-on phase, Sun-Mars radiation rather than Sun-Earth radiation must be determined. All other heat inputs to the hydrogen and the required heating remain the same as for the first power-on phase.

The Mars heating rates were determined in the same manner as the Earth heating rates, except that appropriate values of P and S were used and that radiation form factors were determined at 1.1 Mars radii.

The heat input to the hydrogen for the second power-on phase is summarized in table VII. As for first power-on, additional heat must be added from the reactor to obtain the required heating. Once again, for vehicles 2 and 3, this additional heat is a small amount.

Coast Phase

During the chosen 200- or 230-day coast phase, when the reactor is not in operation, both the heat rate required to vaporize the hydrogen and the nuclear heating obtainable are considerably different from those during the power-on phase. Furthermore, it is assumed that the vehicle is oriented with the payload always facing the Sun during coast and that

solar radiation is not incident on the tank surface. The payload is always between the Sun and the tank, and the payload is assumed to be provided with a temperature-regulating device to maintain its temperature at 520° R. The required and obtained heat inputs to the hydrogen are discussed in the following sections.

Required heating rate. - During coast, or power-off, the heat rate in the reactor, caused by delayed betas and gammas, is given by equation (C14), taken from reference 8 with appropriate notation. If this heat rate $Q_{\beta+\gamma}$ is divided by the change in enthalpy ΔH of the hydrogen as it flows through the reactor, the required flow rate through the reactor $\dot{w}_R$ for afterheat cooling is obtained. The value of Q_{req} varies with coast time, and was calculated for coast times from 30 seconds to the 200 or 230 days selected for the mission (see fig. 14).

Available heating rate. - For the coast phase as for the power-on phase, heat input to the hydrogen occurs from both nuclear and thermal sources:

(1) Nuclear afterheat: The nuclear-afterheat rate was determined by use of equation (C15). The afterheat depends on coast time and was calculated for times from 30 seconds to 230 days.

(2) Thermal heating: The heat inputs to the hydrogen due to thermal radiation from control compartment, conduction through struts from payload to tank, and conduction through conical structure from reactor to tank are the same as those calculated for first power-on phase. Furthermore, vehicle orientation prevents solar heating of the hydrogen. Hence, all heat inputs into the tank are known except the thermal radiation from the payload. The calculation of this quantity involves the determination of the number and spacing of shadow shields (parasols) to be placed on the payload end of the tank so that the sum of the shield weight, shield structure weight, additional required aft transition-piece weight, and the hydrogen boiloff due to thermal radiation from the payload will be a minimum.

(3) Determination of number and spacing of shadow shields on payload end of tank: The number of shadow shields required to protect the tank from thermal radiation from the payload was calculated by the procedure discussed in appendix C. These shields may be made from aluminum foil or from aluminized Mylar. The payload, as stated before, was maintained at 520° R. For that portion of the tank end not shielded from the Sun by the payload, it was assumed that the outermost shadow shield was coated with Al_2O_3 in such a way that the temperature of the portion of this outermost shield was also maintained at 520° R. Under this assumption, for each vehicle, and with the aid of figure 15, the optimum number and spacing of the required shadow shields were found to be eight with $l/d = 0.01$. Figure 16 illustrates this for vehicle 3. For this optimum number and spacing, Q_{pl} was determined by use of figure 15 and

the respective areas to be shielded (367, 307, and 568 sq ft for vehicles 1, 2, and 3, respectively). The sum of Q_{pl} and Q_z then yielded Q_{ob}.

The heat inputs to the tank at the end of coast are given in table VIII to illustrate the magnitudes of the various quantities.

Figure 14 shows plots of both Q_{req} and Q_{ob} against coast time for the three vehicles. The curves show that, for the first few days, a greater heat rate is required than that obtained. Hence, for these first few days, additional heat must be supplied to the hydrogen in the tank by a line from the reactor, or the reactor will melt. After the first few days, this additional heat is cut off, because then Q_{ob} exceeds Q_{req}. Hence, after about 4 to 6 days, some of the vaporized hydrogen is either dumped overboard or more is passed through the reactor with a resulting improvement in cooling, or both.

The possibilities of using closely spaced thermal foils, rather than shadow shields, on the end of the tank facing the payload was also investigated. For the vehicles considered herein, it was found that the use of the optimum number and spacing of shadow shields (eight shields with $l/d = 0.01$) yielded a saving of about 570, 480, and 880 pounds for vehicles 1, 2, and 3, respectively.

SUMMARY OF RESULTS

Of the several shapes studied, the tank shape resulting in the least overall weight was conical for storing the hydrogen used during the spiraling period. An oblate ellipsoid inside the conical tank was found to be a desirable shape for storing the hydrogen used during the second power period. When meteoroid protection is applied to the tanks, the tank weight is increased by as much as about 35 percent for a probability of about 0.92 in the reliability against meteoroid puncture. When protection from meteoroid penetration is not a factor, aluminum was found to be a desirable tank material. Beryllium offers the greatest resistance to meteoroid penetration per unit weight, based on the mechanism for penetration set up herein, as compared with either stainless steel or aluminum. Because the properties of aluminum are better known than those of beryllium, especially at low temperatures, aluminum was chosen for this analytical study.

The heat input to the hydrogen tanks during the boosting period can be reduced to a tolerable amount with about 1/8 inch of fibrous asbestos insulation properly applied.

For each vehicle considered, a heat-rate input to the hydrogen in the tanks, required to cool the reactor and to maintain a constant tank

pressure, was determined for reactor power-on phases. During these phases, nuclear heating far exceeds thermal and solar heating. For materials and equipment having an allowable dose of 10^9 rads, no nuclear shields are required. However, if pumps are used in the hydrogen circuit, nuclear shields weighing 150 pounds are required to meet the heat-input criterion and prevent an undue excess of hydrogen boiloff. When no pumps are used, no nuclear shields are required; in fact, additional heat must be added to the tanks by a line from the reactor in order to obtain the boiloff rate required to cool the reactor and to maintain the constant tank pressure (vehicle 1).

During the 200- or 230-day coast period, the heat input to the tank required for reactor cooling and for maintaining a constant tank pressure varies with coast time. The nuclear afterheating likewise varies with coast time. As coast time increases, the nuclear afterheating gradually dies out, and thermal heating predominates. The number of shadow shields to be placed at the tank end near the payload capsule in order to keep the sum of the hydrogen boiloff due to thermal radiation from the payload, shadow-shield weight, shadow-shield structural weight, and additional required aft transition-piece weight to a minimum was determined for the coast phase. It was found that eight shadow shields with spacing to diameter ratio of 0.01 are required for each vehicle.

For the first few days of coast, the required heat rate exceeds the obtained heat rate. Therefore, during this time additional heat must be added to the tank by a line from the reactor. After about 4 to 6 days of coast, the obtained heat rate exceeds that required. As coast time is increased, the excess vaporized hydrogen must either be thrown overboard or passed through the reactor, thereby maintaining the reactor at a temperature lower than that originally selected.

Lewis Research Center
National Aeronautics and Space Administration
Cleveland, Ohio, November 14, 1960

APPENDIX A

SYMBOLS

A	cross-sectional area, sq cm or sq ft
B	symbolic buildup factor
b	intercept ($t_{Fe} = 0$) of LiH lines on φ_γ/P_R against t_{Fe} plot
b_1	$\sum_{i=1}^{n} (\Sigma_{r,i} t_i)$ or $\sum_{i=1}^{n} (\mu_i t_i)$
C_1	$\frac{\sigma \epsilon \alpha A F}{1 - F^2(1 - \alpha)^2}$
C_2	$C_1 F(1 - \alpha)$
C_3	$\sigma \epsilon A$
c_p	specific heat at constant pressure, Btu/(lb)($^\circ$R)
D	dose rate, rads/hr
d	diameter of inner tank at payload end, ft
E_k	kinetic energy, Btu
E_γ	$0.649\left[(\tau - \tau_0)^{-0.2} - \tau^{-0.2}\right]$, Mev/fission
$E_2(b_1)$	$b_1 \int_{b_1}^{\infty} \frac{e^{-t}}{t^2}\, dt$, (p. 372, ref. 4)
F	radiation form factor (eq. (C8))
F_H	radiation form factor for horizontal surface and spherical planet
F_V	radiation form factor for vertical surface and spherical planet
H	enthalpy, Btu/lb
h	latent heat, Btu/lb

K_f constant (eq. (B3)), Btu/cu in.

K_h constant (eq. (B2)), Btu/cu in.

K_1 constant for conversion from neutrons/(cm^2)(sec) to rads/hr, 10^5

K_2 constant for conversion from photons/(cm^2)(sec) to rads/hr, 2.4×10^5

K_3 average neutron energy, 4.8 Mev/neutron

K_4 average photon energy, 3 Mev/photon

K_5 constant for conversion from Mev/sec to Btu/sec, 1.52×10^{-16}

k thermal conductivity, (Btu)(in.)/(hr)$(ft^2)(^\circ R)$ or Btu/(sec)$(ft^2)(^\circ R/ft)$

L distance between disks used to determine F, in.

L_c reactor-core length, ft

l spacing of shadow shields, ft

N_c number of atoms per cc in homogeneous material

N_i number of atoms per cc in i^{th} material in core

N_{sh} number of shadow shields

n number of hits per 1000 sq ft surface area per day

P planetary heat flux, planet side, Btu/(hr)(sq ft)

P_R reactor power, mw

Q heat rate, Btu/sec

r radius, in.

r_c reactor-core radius, ft

S planetary heat flux, Sun side, Btu/(hr)(sq ft)

S_v source strength of volume source, 1/(cc)(sec)

s distance from Sun, A.U.

T temperature, $^\circ R$

t	thickness, in.
V	volume, cu in. or cu ft
W	specific weight, lb/cu in.
$\dot{w}$	flow rate, lb/sec
Y	probability of success
Z	combined neutron and gamma energies, Mev/(cm^2)(sec)
α	absorptivity
ϵ	emissivity
θ	angle defined in fig. 17
μ_c	absorption coefficient of source material (core), 1/cm
μ_i	absorption coefficient of i^{th} shield, 1/cm
Σ	macroscopic removal cross section, 1/cm
σ	Stefan-Boltzmann constant, 0.1713×10^{-8} Btu/(hr)$(ft^2)(^oR^4)$
σ_i	microscopic cross section, barns
$\tau - \tau_o$	coast time, days
τ_o	power-on time, days
φ_N	neutron flux, neutrons/(cm^2)(sec)
φ_γ	gamma flux, photons/(cm^2)(sec)

Subscripts:

a	afterheat
at	aft transition piece
c	reactor core
cc	control compartment
Fe	iron
f	fusion

H_2	hydrogen
h	heating
I	insulation
LiH	lithium hydride
m	meteoroid
mean	mean
N	neutron
O,γ	gamma, for power-on
ob	obtained
pl	payload
R	reactor
req	required
S	structure
s	struts
sh	shield
ss	stainless steel
T	tank
z	when used with Q, means excess heat into tank before consideration of heat from payload
β	beta
γ	gamma

APPENDIX B

PROCEDURE FOR DETERMINING TANK THICKNESS FOR VARYING DEGREES OF ASSUMED PROTECTION FROM METEOROID DAMAGE

The protection required against meteoritic particles is an undefined, but important, consideration in the design of spacecraft. The size spectrum, flux density, velocity range, and composition of the particles are all speculative items. In spite of the scant information regarding particles in space, an attempt is made herein to explore the possible weight penalties that may have to be imposed on a space vehicle. This attempt may serve to point out the critical areas requiring further data. Because of the speculative nature of this study, requiring many assumptions, a range of protection has been evaluated wherever possible. In this manner the basic weight of the space vehicle (i.e., with no meteoroid protection) is given as well as the weight with varying degrees of protection up to what is at present considered to provide the craft with a large factor of reliability.

Available Data

A table of meteoroid data giving the spectrum of sizes, kinetic energy, and number striking the Earth per day has been assembled by Fred L. Whipple (ref. 9). Portions of the data are given in table III. A large degree of uncertainty exists with all the values in the table, but it is the most commonly accepted compilation at the time of this writing. As discussed in reference 9, the measurable particles compose only about one-fourth of the total spectrum of sizes given in the table. The remainder of the table is an extension of these values that were obtained by visual, photographic, and radio observations. Furthermore, the table assumes that this distribution applies in outer space.

The dimensions of a meteoroid in three perpendicular directions are assumed to be the same. The composition may vary widely from light stony materials, some of which may be very brittle, to heavy metal particles that have a higher compressive strength and melting point than the impacted material. The ratio of brittle stony material to nonbrittle material is controversial. As is stated in the section titled "Effect of Doubling Number of Meteoroid Strikes" in the body of the report and in the next section of this appendix on "Mechanism for Meteoroid Penetration," an assumption that one-half the meteoroids are nonbrittle was made for this study. The results of this assumption are compared with those for an assumption that all meteoroids are nonbrittle in order to obtain an indication of the maximum weight penalty for a safe design.

Mechanism for Meteoroid Penetration

The action of a meteoroid impacting on the skin of a spacecraft tank is not known. Some writers hold that brittle material is less of a problem than nonbrittle material. Some structural protective concepts involve a "bumper" guard surrounding the structure to be protected (ref. 9). The suggested mechanism is that the brittle material will shatter upon impact with the thin guard, and the fragments penetrating the guard will be very small. By further reasoning, the statement is made that these small fragments can be dealt with more easily than the original larger one-piece meteoroid. This reasoning is questioned by an experiment performed at the Lewis Research Center in which glass projectiles were shot at about 6000 feet per second at a 0.010-inch-thick sheet of stainless steel. A plug sheared from the thin sheet by the projectile impacted upon the target with a consequent damage considered as bad as a direct impact by the original projectile. Since none of the experiments duplicate the conditions thought to exist in space, as regards brittleness, speed, and low density of the projectile, the question remains unanswered to any degree of satisfaction.

The manner in which the meteoroid will damage a vehicle structure is thought to be better understood for the nonbrittle meteoroids than for the brittle type. Some investigators (see ref. 10) have attempted to relate the penetration of hypervelocity (over about 5000 ft/sec) metal projectiles into the target with the ratio of the projectile velocity to the speed of sound in the target material. The estimated velocities of meteoroid impact may vary from 50,000 to 100,000 feet per second (see table III), which are generally higher than the speed of sound in the structural material of the space vehicle (speed of sound in Al = 16,750 ft/sec, steel = 16,410 ft/sec, beryllium = 42,170 ft/sec, Cu = 11,670 ft/sec). Although the fundamental principles governing the mechanism of penetration of hypervelocity projectiles are not understood well enough to explain experimental observations completely or to forecast damage caused by a meteoroid, agreement exists among many experimenters using guns firing at velocities of about 13,000 feet per second that the kinetic energy of the projectile is absorbed by the melting action of the target and perhaps the projectile material.

As shown in reference 10, the impacts form craters in the target. The shape of the craters is important in determining material thickness required to absorb the energy of the meteoroid. A study of the craters indicates a nearly hemispherically shaped crater for projectiles with a velocity higher than the velocity of sound in the target material.

Assumptions

The penetration calculations that follow were guided by the following assumptions:

(1) The colliding meteoroid produces a hemispherical crater beginning at the point of impact and enlarging until either all the meteoroid kinetic energy is absorbed as shown in figure 5(a) or the crater has enlarged sufficiently to permit penetration of the meteoroid through the wall (fig. 5(b)).

(2) The kinetic energy of the meteoroid is absorbed by (a) the heat required to raise the temperature of the material affected from 45° R to its melting point, and (b) the heat of fusion of the material affected.

(3) The probability of a space vehicle's colliding with a meteoroid is determined from table III from the values of the estimated strikes on the Earth's atmosphere. This value is given in the table as the number of meteoroids of any given size striking a 1000-square-foot surface per day. The number of expected collisions is directly proportional to the area of the vehicle and the number of days of exposure. For any meteoroid visual magnitude listed in table III, the number striking the 1000-square-foot surface area per day includes all bodies of weight greater than the number indicated for the visual magnitude in question.

(4) One-half the number of strikes listed in the last column of table III is assumed composed of nonbrittle meteoroids for all the sizes and strikes. The results are compared with the assumption that all the strikes listed in table III are nonbrittle. Future space data on this factor will determine what proportion of the weight penalty for meteoroid protection given herein is applicable.

(5) "Bumper" guards are used herein only insofar as these guards serve as shields or structures for other purposes. When the assumption that meteoroids do not shatter upon impact but rather melt hemispherical craters is made, a single thick sheet is more advantageous than multiple sheets of thinner material, because the volume of crater created (thus, kinetic energy absorbed) increases as the cube of the radius of the crater.

Stepwise Procedures

The following stepwise procedure is used for determining the wall thicknesses for varying degrees of protection; that is, for varying assumed probabilities of not being punctured:

Step A. - The design probability Y of a successful mission is established. For this illustrative example, a value of $Y = 0.95$ or larger is desired.

Step B. - The area to be protected and the number of days exposed to the meteoroids are determined. For this example, the area exposed to possible meteoroid damage is 326 square feet, and it is exposed for 230 days.

Step C. - The number of hits per thousand square feet of surface area per day n that can be tolerated for the desired probability established in step A is found from the expression

$$n\left(\frac{\text{Area}}{1000}\right)(\text{Days}) = 1 - Y \tag{B1}$$

For this example, $n = 6.7\times10^{-4}$.

Step D. - The meteoroid magnitude that has been established by Whipple as striking an area of 1000 square feet per day the same number of times as determined by n in step C is found from table III. According to the first and last columns of table III, meteoroids of magnitude 8 strike an area of 1000 square feet 6.72×10^{-4} time per day. If it is assumed that one-half the strokes listed in the table cause no damage, one-half the meteoroids of magnitude 9 strike an area of 1000 square feet 8.5×10^{-4} time per day. This value is the nearest value to n found in step C.

Step E. - From table III the kinetic energy E_k associated with the meteoroid of magnitude chosen is noted. For this example, the value of kinetic energy is 5.56 Btu for a meteoroid magnitude of 8 and 2.06 for a magnitude of 9.

Step F. - The volume of wall material that must be melted in order to absorb the kinetic energy of the meteoroid is determined. The energy absorption takes place in two steps:

(1) Heating the material from ambient temperature to the melting point

$$E_{k,h} = VWc_p\Delta T = VK_h \tag{B2}$$

(2) Heat of fusion at the melting point

$$E_{k,f} = VWh = VK_f \tag{B3}$$

The total volume required to absorb the kinetic energy of the meteoroid is

$$V = \frac{E_k}{K_h + K_f} \tag{B4}$$

The values of $K_h + K_f$ for steel, aluminum, and beryllium are 131, 52.7, and 117, respectively. The ambient temperature is assumed to be 45° R.

Step G. - The sheet thickness t is calculated in which a hemispherical crater with the volume determined in step F can be formed with a depth equal to the sheet thickness. For this example and for aluminum as the material,

$$V = \frac{2.06}{52.7} = \frac{2}{3}\pi t^3$$

$$t = 0.266 \text{ in.}$$

The procedure in this step for determining the sheet thickness must be modified with an intermediate step if another wall acting as a protective barrier is in front of the wall under consideration. This condition exists with respect to the inner tank with the outer tank acting as a protective barrier to some extent. For aluminum as the tank wall material, the kinetic energy absorbed by the outer tank when the meteoroid penetrates as shown in figure 5(b) is

$$E_{k,x} = (52.7)\left(\frac{1}{3}\pi t_x\right)\left(3r_m^2 + t_x^2\right) \tag{B5}$$

where r_m is the meteoroid radius obtained from table III. The difference between the original kinetic energy E_k in the meteoroid (2.06 Btu in this example) and the energy $E_{k,x}$ absorbed in the outer wall is the energy that must be absorbed by the inner wall by melting a hemispherical crater.

Effect of Meteoroid Penetration on Tank Failure

Because of the very high meteoroid velocities, a meteoroid hit will cause an almost instantaneous change in stress surrounding the point of impact. The tank material will therefore behave as brittle regardless of the ductility it may have at liquid-hydrogen temperatures. The effect of the local increase in temperature at the point of impact is difficult to evaluate theoretically because of the number of interrelated factors present. The melting of metal at the point of impact will tend to relieve stress concentrations, but would also give rise to thermal stresses. These thermal stresses depend upon the rate of temperature rise, the dissipation of heat into the tank and liquid hydrogen, and the properties of the tank material.

According to reference 11, the stress-concentration factor for a circular hole in a flat plate is 2.5. The stress-concentration factor cited is based on a cylindrical hole penetrating the wall completely; whereas, according to the mechanism considered herein, the meteoroid crater is hemispherical with the bottom of the crater tangent to the inside surface as the limiting condition for failure. The hemispherical

crater does not remove as much metal as the cylindrical hole; furthermore, part of the removed metal from the crater will weld as a boss around the rim. The ratio of volume of metal removed by the hemispherical crater to the volume of metal removed by a right circular cylinder is 2/3. Whether the stress-concentration factor around the hemispherical crater is 2/3 the value of the stress-concentration factor around a right circular hole through the plate is not known and should be a subject of further investigation. For this simple analysis, the stress-concentration factor around a hemispherical crater is assumed to be approximately 1.7.

A value of 60,000 psi was used as the design stress for the aluminum tanks in this study. The ultimate strength of aluminum at liquid-hydrogen temperature is 93,000 psi (see ref. 12), thus permitting a stress concentration of 1.55 before failure based only on the ratio of ultimate strength to design stress. The assumption that the limiting condition of failure is when the crater bottom is tangent with the inside tank surface further assumes a small amount of help in reducing the stress concentration from the boss welded around the rim of the crater and from stress relief during the melting of the crater.

The preceding simple analysis presumes that the tank wall was stressed to 60,000 psi by the internal pressure force before the crater was formed. When the tank wall thickness is increased for meteoroid protection beyond the minimum required by the pressure force, the design is no longer marginal with respect to the stress concentration due to meteoroid craters. This condition exists when the inner aluminum tank containing the hydrogen during the coasting period is designed for a probability of a successful trip of over 0.7.

APPENDIX C

HEAT INPUT TO HYDROGEN

The analytical procedures used to determine the various rates of heating of the hydrogen in the tanks during both reactor power-on and coast periods are described in this appendix. In addition, procedures for determining the thicknesses and weights of the nuclear shield and the number of shadow shields (parasols) required at the payload end of the tank are included. Finally, a design procedure is suggested.

Power-On Phase

Nuclear heating. - Correlation of nuclear heating and dose rate: For a given reactor power P_R, the neutron and gamma fluxes φ_N and φ_γ can be determined by the method discussed in appendix D for any given combination of assumed neutron- and gamma-shield thicknesses. The dose rate can be expressed by

$$D = \frac{\varphi_N}{K_1} + \frac{\varphi_\gamma}{K_2}, \text{ rads/hr} \tag{C1}$$

where K_1 and K_2 are conversion constants for converting neutron and gamma fluxes into dose rates; $K_1 = 10^5$ and $K_2 = 2.4 \times 10^5$. Moreover, the heating rate at the point exterior to the shield where the fluxes are determined (see fig. 17) can be obtained from

$$\frac{Q}{A_{sh}} = (K_3\varphi_N + K_4\varphi_\gamma)K_5, \text{ Btu/sq cm} \tag{C2}$$

where K_3 and K_4 (4.8 and 3, respectively) denote the average assumed energies of neutrons and gammas, K_5 (1.52×10^{-16}) converts Mev per second to Btu per second, and A_{sh} is the cross-sectional area (sq cm) at the exterior side of the gamma shield where the fluxes have been determined.

Elimination of φ_N from equations (C1) and (C2) results in an expression between D/φ_γ and $Q/A_{sh}\varphi_\gamma$. Now, φ_γ in turn is a function of reactor power and of neutron- and gamma-shield thicknesses, t_{LiH} and t_{Fe}, respectively. For any chosen thickness of neutron shield and of reactor power, a relation between φ_γ, power, and gamma-shield thickness results; it is

$$\varphi_\gamma = b_{LiH} P_R e^{-0.639 t_{Fe}} \tag{C3}$$

where b_{LiH} is the value of φ_γ/P_R for $t_{Fe} = 0$, and -0.639 is the slope obtained from a plot of equation (C3) on semilog paper for a range of values of the variables. The value of b varies as t_{LiH} varies. Finally, by inserting equation (C3) into the equation resulting from the elimination of φ_N between equations (C1) and (C2), by employing the values of the constants as listed, and by reducing the result to unit power, the following relation is obtained:

$$\frac{D}{P_R} = (1.37\times10^{10})\frac{Q}{A_{sh}P_R} - (2.083\times10^{-6})b_{LiH}e^{-0.639t_{Fe}}, \text{ rads/(hr)(mw)} \tag{C4}$$

Nuclear shield weight: The weights of the nuclear shield were obtained by approximating each shield as a cylinder whose height was the shield thickness and whose radius was the mean radius of the respective shield. The volumes of the cylinders were multiplied by the densities (0.79 g/cc for LiH and 7.8 g/cc for Fe) and divided by 454 to obtain shield weight in pounds.

Nuclear heating rate: The nuclear heating rate is obtained by converting the neutron and gamma fluxes to energy (i.e., calculating $4.8\varphi_N$ and $3\varphi_\gamma$) and summing to obtain the combined neutron and gamma energies Z (Mev/(cm^2)(sec)). Multiplication by the cross-sectional area A_{sh} at the point where the fluxes are calculated and conversion to Btu per second then yield the following:

$$Q_{\gamma+N} = ZA_{sh}\,(1.52\times10^{-16}), \text{ Btu/sec} \tag{C5}$$

The gamma heating rate, needed for coast calculations to be discussed later, can be obtained from $Q_{\gamma+N}$ as follows:

$$Q_{O,\gamma} = \left(\frac{3\varphi_\gamma}{Z}\right) Q_{\gamma+N}, \text{ Btu/sec} \tag{C6}$$

Thermal heating. - Thermal radiation from control compartment to tank: Calculation of this heat rate into the tank can be accomplished by application of the method developed in reference 7. For use herein, the case of no thermal shields between the control-rod compartment and the tank was considered. The heat rate, according to the reference, can then be expressed as

$$Q = C_1T_{cc}^4 + (C_2 - C_3)\,T_I^4 = \frac{k_I}{t_I}(T_I - T_{H_2})A_T \tag{C7}$$

For calculation purposes, it was assumed that a 1-inch layer of insulation surrounded the tank, and that this insulation had a thermal conductivity $k_I = 0.11$ (Btu)(in.)/(hr)(ft^2)($^\circ$R). In addition, it was assumed that the control compartment was maintained at room temperature (520° R) and that the hydrogen in the tank was maintained at 45° R. Although the end of the control compartment facing the tank is of a smaller diameter than the tank end near it, and although the tank end near it is ellipsoidal, it is assumed that the geometry can be represented by two disks whose radii are the same (equal to the larger radius at the tank end near the control compartment). Then the radiation form factors necessary for determination of C_1 and C_2 were calculated from

$$F = 1 - \frac{1}{2}\left(\frac{L}{r}\sqrt{4 + \frac{L^2}{r^2}} - \frac{L^2}{r^2}\right) \qquad (C8)$$

where L is the distance between the two disks (ref. 13). Values of $\alpha = 0.1$ and $\epsilon = 0.1$ were also assumed.

Conduction through struts from payload to tank: Eight 1-inch-diameter struts were assumed to connect the payload to the tank. Assuming the separation distance between payload and tank to be 12 inches, and assuming the payload maintained at room temperature (520° R) and the hydrogen in the tank at 45° R, the heat rate was calculated from the standard conduction equation,

$$Q = \frac{k_s A_s}{3600\ t_s}(T_{pl} - T_{H_2}),\ \text{Btu/sec} \qquad (C9)$$

A stainless-steel strut with thermal conductivity of 5.8 Btu/(hr)(ft)($^\circ$R) was assumed; 1 percent of this value was used for k in the equation, as stated in the text.

Conduction through conical structure from reactor to tank: A conical shell of stainless steel 0.020 inch thick was assumed. The standard conduction equation (C9) also applies here. A reactor temperature T_R (which replaces T_{pl} in the equation) of 1000° R was used for this calculation. The distance t in this case is the slant height of the cone, from reactor to tank. A value of $k_s = k_{ss} = 5.8$ Btu/(hr)(ft)($^\circ$R) was again assumed.

Thermal radiation from payload to tank: At this point, all the thermal heat rates into the tank except that from the payload are known, and the heat rate required for both reactor cooling and the maintenance of a constant tank pressure can be determined. (This will be explained in the section "Procedure for Choice of Shields.") To keep the thermal radiation from the payload at a reasonable value, thermal foils or

shadow shields are placed on the tank end nearest the payload. Because the nuclear heating for power-on is so large, the heat rate from payload to tank is negligible in comparison. Therefore, for power-on, shadow shields are not necessary to protect the tank from the payload. During coast, the heat rate from the payload is significant, and shadow shields are required. The method of determining the number and spacing of these shields will be discussed in the section "Coast Phase."

Other sources of heat: The method for the development of equations for use in calculating Sun-Earth and Sun-Mars radiation is discussed in reference 7. The assumptions employed in such an analysis are also given in the reference. The hydrogen tank is assumed to be replaced by a cubical tank of equivalent volume in order to simplify the calculations. The tank is assumed to be coated with a material such as Al_2O_3; then $\alpha = 0.168$ and $\epsilon = 0.77$ can be assumed (ref. 14). Insulation thickness and conductivity are the same as those used previously. The following equations result from the method of reference 7:

Tank side near Earth:

$$\frac{Q}{A} = \alpha F_H P - \sigma \epsilon T_I^4 = \frac{k_I}{t_I} (T_I - T_{H_2}), \text{ Btu/(hr)(sq ft)} \qquad (C10)$$

Tank side near Sun:

$$\frac{Q}{A} = \alpha S - \sigma \epsilon T_I^4 = \frac{k_I}{t_I} (T_I - T_{H_2}), \text{ Btu/(hr)(sq ft)} \qquad (C11)$$

Each vertical side of tank:

$$\frac{Q}{A} = \alpha F_V P - \sigma \epsilon T_I^4 = \frac{k_I}{t_I} (T_I - T_{H_2}), \text{ Btu/(hr)(sq ft)} \qquad (C12)$$

For a unit area normal to a radius vector from the Sun, the incident solar flux is inversely proportional to the square of the distance from the Sun and is given by

$$\frac{Q}{A} = \frac{427.5}{s^2}, \text{ Btu/(hr)(sq ft)} \qquad (C13)$$

where s is the distance from the Sun in astronomical units (see ref. 7). From equation (C13), the planetary heat flux S on the tank side near the Sun at the Earth's distance from the Sun equals 427.5 Btu/(hr)(sq ft). The heat received from a planet is composed of thermal radiation from the planet due to its temperature and that portion of the Sun's heat energy that is reflected from the planet. The planetary heat flux on the tank side at the Earth's surface P equals 250 Btu/(hr)(sq ft).

Definitions of the form factors between a horizontal surface and a spherical planet and between a vertical surface and a spherical planet are given by equations (C2) and (C3) of reference 7. These vary with distance from the planet surface to the tank surface; for calculation purposes, average values were obtained at selected altitudes and used as constants.

Equations (C10), (C11), and (C12) may also be used to determine Sun-Mars radiation. The values of S and P for Sun-Mars radiation are S = 182 and P = 129 Btu/(hr)(sq ft). Values of F_H and F_V were determined for 1.1 Mars radii.

Coast Phase

Nuclear heating. - During coast or power-off time, the heat given up by the reactor is that caused by the emission of beta and gamma energy from the fission products after shutdown. According to equation (2.182.1) of reference 8, this heat rate can be expressed by

$$Q_{\beta+\gamma} = 5.59353\ P_R\left[(\tau - \tau_0)^{-0.2} - \tau_0^{-0.2}\right] \text{Btu/sec} \qquad (C14)$$

where $\tau - \tau_0$ is coast time in days, τ_0 is power-on time at Earth in days, and where units have been converted to be consistent with those used herein. The heat rate $Q_{\beta+\gamma}$ is calculated for various coast times from 30 seconds to either 200 or 230 days, the trip time selected for the mission. Since equation (C14) is valid only after 10 seconds, and since an abrupt shutdown of the reactor is not possible, a conservative lower limit of 30 seconds was chosen for afterheat calculations. This reactor heat rate is required, as will be explained later, to find the reactor required flow rate during coast.

Nuclear afterheat: The nuclear afterheat rate of hydrogen heating can be calculated from the relation

$$Q_a = \frac{E_\gamma}{15} Q_{0,\gamma}, \text{ Btu/sec} \qquad (C15)$$

where 15 Mev = five 3-Mev gammas per fission is the assumed average energy,

$$E_\gamma = 0.649\left[(\tau - \tau_0)^{-0.2} - \tau^{-0.2}\right], \text{ Mev/fission} \qquad (C16)$$

and $Q_{0,\gamma}$ is given by equation (C6) and represents the gamma heating in the reactor for power-on condition.

Thermal heating. - During coast, it is assumed that the vehicle will be oriented so as to prevent solar heating of the hydrogen. The thermal

radiation from the control compartment to the tank, the conduction through struts from payload to tank, and the conduction through the conical structure from reactor to tank are the same for coast as for power-on; these have already been discussed for power-on.

Thermal radiation from payload to tank: During coast, the heat rate required for cooling the reactor and for maintaining a constant tank pressure can be determined by the method to be discussed in "Procedure for Choice of Shields." If this heat rate is subtracted from the sum of (1) the nuclear afterheat, (2) the thermal radiation from the control compartment, (3) the conduction through the struts from the payload, and (4) the conduction through the conical structure from the reactor to the tank, the heat rate in excess of that required is obtained; call this Q_z. The heat rate per unit area per day entering the tank for an assumed l/d ratio and an assumed number of shadow shields can be read from figure 15. If this quantity is multiplied by the area of the tank to be shielded and by 194.27 (the latent heat of vaporization of hydrogen used in the preparation of fig. 15), and divided by the number of seconds in a day, the heat rate from the payload Q_{pl} for the assumed l/d ratio and number of shadow shields is obtained. The objective is to determine the number and spacing of shadow shields that will result in a minimum for the sum of the weights of the shadow shields, the shadow-shield structure, the hydrogen boiloff due to thermal radiation from the payload, and the aft transition piece (which depends upon the number and spacing of the shadow shields).

For an assumed l/d ratio and an assumed number of shadow shields, the quantities just mentioned whose sum is to be minimized can be found as follows:

(1) Shadow-shield weight: Assuming shadow shields weigh approximately 0.07 pound per square foot per shield, calculate $W_{ss} = (0.07)(\text{Area of tank to be shielded})N_{sh}$.

(2) Shadow-shield structural weight: Assuming the structure is made of nylon, which weight will be 28.8 pounds per foot, and allowing a 10-percent increase for a shadow-shield erection device, calculate $W_S = 28.8\ (1.1)(l)(N_{sh} + 1)$.

(3) Weight of hydrogen boiloff: Calculate W_{H_2} = (reading from fig. 15)(194.27/165)(Days)(Area of tank to be shielded).

The 194.27 is the latent heat of vaporization of hydrogen used in the preparation of figure 15, and 165 is the latent heat of vaporization of hydrogen used herein.

(4) Weight of aft transition piece: Calculate
$W_{at} = \left(\frac{\text{wt.}}{\text{ft}} \text{ of aft transition piece}\right)(l)(N_{sh} + 1)$.

The sum of the four items is calculated for various assumed values of l/d and number of shadow shields, and the minimum sum then yields both the number of shadow shields and their spacings. This is illustrated for vehicle 3 in figure 16. This same number of shadow shields will be present for the entire mission and hence must be included for power-on as well as coast.

E-3/4

Depending upon the number of shadow shields and the spacings determined, lengthening the struts between the payload and tank, and hence recalculating the conduction through the struts, may be required. An iterative process may be required before a conclusive answer results.

The excess heat rate into the tank can be found by adding Q_{pl} and Q_z. From this, the excess boiloff of hydrogen is obtainable by integrating over the coast period and dividing by the latent heat of vaporization of hydrogen at the tank conditions.

Procedure for Choice of Shields

Nuclear shield. - The determination of the nuclear shield, which of necessity must be calculated for power-on, will be discussed first. The reactor size and power must be known, and a total allowable dose in rads is assumed. The power-on time at Earth is obtained from the trajectory calculation of the vehicle for the specific mission chosen. Then the dose rate D in rads per hour can be calculated, and D/P_R can be determined. From figure 11, corresponding to this value of D/P_R, values of t_{Fe}, t_{LiH}, and $Q/A_{sh}P_R$ can be read. For each combination of t_{Fe} and t_{LiH}, the cross-sectional area at the exterior face of the shield can be calculated. Hence, corresponding to D/P_R, a series of t_{Fe}, t_{LiH}, $Q/A_{sh}P_R$, and A_{sh} is now known.

The next step is to determine the value of $(Q/A_{sh})_{req}$ required to cool the reactor and to maintain a constant pressure in the hydrogen tank. The flow rate through the reactor can be found from

$$\dot{w}_R = \frac{0.95(948.1)P_R}{\Delta H}, \text{ lb/sec} \qquad (C17)$$

where ΔH is the enthalpy change of the hydrogen as it flows through the reactor and changes its temperature from T_{in} to T_{out}. When liquid

hydrogen is withdrawn from the tank for use in the reactor, the void in the tank must be filled with vaporized hydrogen. Now, the density ratio of liquid to vaporized hydrogen is 3.9/0.3, or 13. Hence, the flow rate necessary to fulfill the reactor cooling requirements and to maintain a constant tank pressure becomes $\dot{w}_R\left(1 + \frac{1}{13} + \frac{1}{13^2} + \ldots\right)$ where the successive terms in the series represent hydrogen vapor required to replace the voids created by the liquid-level decrease. At this point two cases must be considered: (1) The reactor acts as a boiler and no pumps are used in the flow system, and (2) pumps are used and liquid hydrogen is flowing through the pumps. In the first case, the required flow rate is that stated before; the series can be summed and there is obtained $(13/12)\dot{w}_R$ as required flow rate. If pumps are used, liquid hydrogen is withdrawn from the tank; the required vaporization then applies only to filling the voids in the tank. Hence, the term unity is no longer required in the parentheses, and the required flow rate becomes $(1/12)\dot{w}_R$. Multiplication of these respective flow rates by the latent heat of vaporization of the hydrogen (at 45° R and 50 psi), namely, 165 Btu per pound, yields the required value of Q (Q_{req}). Now, Q_{req} is divided by each of the previously calculated areas, and $Q_{req}/A_{sh}P_R$ is obtainable. A plot of $(Q/A_{sh}P_R)_{curve}$ divided by $Q_{req}/A_{sh}P_R$ against t_{Fe} can now be made, and values of t_{Fe} for unit values of the ordinate are possible shield solutions. For each such value of t_{Fe}, and the known value of D/P_R, corresponding values of t_{LiH} can be read from figure 11. Finally, with the corresponding values of t_{Fe} and t_{LiH}, the shield weights can be read from figure 12. The combination of two thicknesses (t_{Fe} and t_{LiH}) that yields the minimum shield weight is the one desired. This procedure is applicable if the nuclear radiation is the criterion that must be met.

In some cases, the heat input into the tank, rather than the nuclear radiation, is the dominating criterion. By choosing values slightly less than the known required heat inputs and using the reactor powers and assumed approximate shield cross-sectional areas, approximate values of $Q/A_{sh}P_R$ can be obtained. Corresponding to these values, values of D/P_R and a series of shield thicknesses (each of which would satisfy the requirements) can be read from figure 11. Shield weights corresponding to these various acceptable shield thicknesses can be read from figure 12. The lightest-weight shield is the one desired.

Thermal shields. - The number of shadow shields required at the payload end of the tank is determined for coast, as stated before. Division of equation (C14) by ΔH yields the value of $\dot{w}_R$. For coast, the pumps

are not in operation, and so for all cases the flow rate required for both cooling requirements and the maintenance of a constant tank pressure is $(13/12)\dot{w}_R$. Multiplication by 165 Btu per pound, the latent heat of vaporization of the hydrogen in the tank at the assumed conditions, yields the required heat rate Q_{req}. The procedure for determining the number and spacing of shadow shields now follows as explained in the section "Coast Phase" under "Thermal heating."

APPENDIX D

CALCULATIONS OF SHIELDING NECESSARY TO PREVENT RADIATION DAMAGE TO REACTOR CONTROL EQUIPMENT

By John M. Smith

Calculations were made to evaluate shielding required to keep the radiation dose in the reactor control compartment below a limiting value. A shield consisting of lithium hydride and iron would be located at the reactor end of the control compartment. Figure 17 shows the reactor and the position of the shielding materials. A total allowable dose in the control compartment was set at 10^9 rads.

The advanced reactor concept and reactor materials discussed in reference 3 were adapted for this study; that is, the reactor is assumed to contain tungsten, uranium dioxide, beryllium oxide, and beryllium. The size of the cylindrical core was estimated as discussed briefly in reference 2. The number of atoms per cubic centimeter of each material was found from the calculations for a heterogeneous reactor. Using the microscopic removal cross sections for neutrons listed in table IX, the macroscopic removal cross section of the reactor core was found to be the summation of $N_i\sigma_i$, where N_i is the number of atoms per cubic centimeter and σ_i (cm^2 or barns) is the microscopic cross section of each material in the core. The values of the microscopic cross sections were taken from reference 15 (table II, p. 22).

The gamma absorption coefficient of the core was found to be the summation of $(N_i/N_c)\mu_i$, where N_i has just been defined, N_c is the number of atoms per cubic centimeter in the homogeneous material, and μ_i is the total gamma absorption coefficient for the homogeneous material at an average energy of 3 Mev. The values of μ_i were taken from curves in reference 16 (pp. 11 to 41).

For the shielding materials used, the macroscopic removal cross section of lithium hydride was found to be 0.116 per centimeter, and that for iron to be 0.167 per centimeter. These values were calculated by using the microscopic removal cross-section values from table IX. The density for lithium hydride was taken as 0.79 gram per cubic centimeter. The gamma absorption coefficient for lithium hydride was found to be 0.028 per centimeter, and that of iron to be 0.270 per centimeter. The value of μ for lithium hydride was found by using microscopic cross sections listed in reference 17. The value of μ for iron at 3 Mev was taken from values listed in reference 16 (p. 22).

A series of calculations was made for different thicknesses of lithium hydride and iron to find values of the fast-neutron flux φ_N and the gamma flux φ_γ at a point on the centerline just outside the iron shield in the control compartment.

The following equation was used assuming a cosine distribution of the leakage of neutrons and gammas out of the end surface of the reactor. This equation gives the value of the flux along the centerline outside a given shield. The equation is taken from reference 4 (p. 364). For the neutron-flux calculation, because the iron is not followed by a hydrogenous material, the removal cross sections do not apply. Ordinarily, removal cross sections, when applicable, account for scattered radiation, and no buildup factor is required. Across the iron, therefore, a combination of exponential attenuation and buildup was used. The buildup factor was assumed to be $1 + \Sigma_{Fe}t_{Fe}$, where Σ_{Fe} is the macroscopic removal cross section for iron and t_{Fe} is the iron thickness.

For neutrons, the equation is

$$\varphi_N = \frac{B_N S_{v,N}}{2\Sigma_c}\left[E_2(b_1) - \frac{E_2(b_1 \sec \theta)}{\sec \theta}\right] \qquad (D1)$$

where the volume source strength of neutrons $S_{v,N}$ is equal to $(3.1\times10^{16})(P_R)(2.5)/V_c$; 3.1×10^{16} is the number of fissions per second per megawatt; 2.5 is the average number of neutrons per fission; b_1 is the summation of $\Sigma_{r,i}t_i$, where $\Sigma_{r,i}$ is the removal cross section and t_i is the thickness of each shielding material; and $E_2(b_1) = b_1 \int_{b_1}^{\infty} \frac{e^{-t}}{t^2}\,dt$, values of which are found in reference 4 (p. 372).

For the gamma flux,

$$\varphi_\gamma = \frac{B_\gamma S_{v,\gamma}}{2\mu_c}\left[E_2(b_1) - \frac{E_2(b_1 \sec \theta)}{\sec \theta}\right] \qquad (D2)$$

where B_γ is the buildup factor for collided gammas and is found from a curve for buildup in iron in reference 16 (p. 49), where b_1 is the abscissa and the average energy assumed is 3 Mev; $S_{v,\gamma}$ is the volume source strength of gamma photons (it is assumed that five 3-Mev gammas are emitted per fission so that $S_{v,\gamma} = 2S_{v,N}$); and b_1 is the summation of $\mu_i t_i$, where μ_i is the total absorption coefficient and t_i is the thickness of each shielding material.

After calculating φ_N and φ_γ, these values were converted to dose rate in rads per hour using conversion factors (see appendix A), assuming an average energy of 3 Mev per gamma and $2\frac{1}{2}$ Mev per neutron.

REFERENCES

1. Cavicchi, Richard H., and Miser, James W.: Determination of Nuclear-Rocket Power Levels for Unmanned Mars Vehicles Starting from Orbit About Earth. NASA TN D-474, 1962.

2. Ellerbrock, Herman H., Cavicchi, Richard H., Duscha, Rudolph A., and Linke, Heinz G.: Systems Design of Unmanned Nuclear-Powered Mars Vehicles Starting from Orbit About Earth. NASA TM X-486, 1962.

3. Rom, Frank E., and Johnson, Paul G.: Nuclear Rockets for Interplanetary Propulsion. SAE Trans., vol. 68, 1960, pp. 600-609.

4. Rockwell, Theodore, III, ed.: Reactor Shielding Design Manual. TID-7004, AEC, Mar. 1956.

5. Kramer, John L., Lowell, Herman H., and Roudebush, William H.: Numerical Computations of Aerodynamic Heating of Liquid Propellants. NASA TN D-273, 1960.

6. Scott, Russell B.: Cryogenic Engineering. D. Van Nostrand Co., Inc., 1959.

7. Smolak, George R., and Knoll, Richard H.: Cryogenic Propellant Storage for Round Trips to Mars and Venus. Aero/Space Eng., vol. 19, no. 6, June 1960, p. 42.

8. Glasstone, Samuel: Principles of Nuclear Reactor Engineering. D. Van Nostrand Co., Inc., 1955.

9. Whipple, Fred L.: The Meteoritic Risk to Space Vehicles. Paper 499-57, Am. Rocket Soc., 1957.

10. Charters, A. C., and Locke, G. S., Jr.: A Preliminary Investigation of High-Speed Impact. The Penetration of Small Spheres into Thick Copper Targets. NACA RM A58B26, 1958.

11. Peterson, R. E.: Stress Concentration Design Factors. John Wiley & Sons, Inc., 1953.

12. Hanson, M. P., Stickley, G. W., and Richards, H. T.: Sharp-Notch Behavior of Some High-Strength Sheet Aluminum Alloys and Welded Joints at 75, -320, and -423° F. Symposium on Low Temperature Properties of High Strength and Missile Materials, ASTM, Atlantic City (N.J.), June 26-July 1, 1960.

13. Leuenberger, H., and Person, R. A.: Compilation of Radiation Shape Factors for Cylindrical Assemblies. Paper 56-A-144, ASME, 1956.

14. Olson, O. Harry, and Morris, James C.: Determination of Emissivity and Reflectivity Data on Aircraft Structural Materials. Pt. III - Techniques for Measurement of Total Normal Emissivity, Normal Spectral Emissivity and Presentation of Results. TR 56-222, WADC, Jan. 1959.

15. Chapman, G. T., and Storrs, C. L.: Effective Neutron Removal Cross Sections for Shielding. AECD-3978, AEC, Sept. 19, 1955.

16. Moteff, John: Miscellaneous Data for Shielding Calculations. Apex 176, Aircraft Nuclear Prop. Dept., Atomic Products Div., General Electric Co., Dec. 1, 1954.

17. Storm, Ellergy, Gilbert, Eugene, and Israel, Harvey: Gamma Ray Absorption Coefficients for Elements 1 through 100 Derived from the Theoretical Values of the National Bureau of Standards. LA 2237, Los Alamos Sci. Lab., Nov. 18, 1958.

TABLE I. - COMPARISON OF THREE VEHICLE CONCEPTS

Vehicle		1	2	3
Power, mw		25	150	400
Hydrogen volume for escape, cu ft		4445	3335	8219
Hydrogen volume stored during coasting period, cu ft		880	710	1764
Length of tank plus supporting structure, ft (m)	Two spheres	68 (20.7)	61 (18.6)	83 (25.3)
	Cluster of spheres	60 (18.3)	59 (18.0)	83 (25.3)
	Cone	51 (15.5)	47 (14.3)	65 (19.8)
Weight of tanks, lb (kg)	Two spheres	2775 (1259)	2284 (1036)	5800 (2631)
	Cluster of spheres	2699 (1224)	2297 (1042)	5796 (2629)
	Cone	3400 (1542)	2700 (1225)	7140 (3239)
Weight of supporting structure, lb (kg)	Two spheres	1044 (473)	960 (435)	2720 (1234)
	Cluster of spheres	1340 (608)	1340 (608)	2720 (1234)
	Cone	300 (136)	300 (136)	300 (136)
Weight of tank plus structure, lb (kg)	Two spheres	3819 (1732)	3244 (1471)	8520 (3865)
	Cluster of spheres	4039 (1832)	3637 (1650)	8516 (3863)
	Cone	3700 (1678)	3000 (1361)	7440 (3375)

TABLE III. - ASSUMED SPECTRUM OF METEOROID CONDITIONS IN SPACE

Meteor visual magnitude	Weight		Radius, r_m		Assumed velocity		Kinetic energy, E_K		Cumulative number striking 1000 sq ft surface area per day
	lb	kg	in.	cm	ft/sec	km/sec	ft-lb	Btu	
0	5.51×10^{-2}	2.50×10^{-2}	1.94	4.93	91,840	28	7.38×10^{6}	9.48×10^{3}	
1	2.19×10^{-2}	$.99\times10^{-2}$	1.43	3.63			2.94×10^{6}	3.77×10^{3}	
2	8.73×10^{-3}	3.96×10^{-3}	1.05	2.67			1.16×10^{6}	1.59×10^{3}	
3	3.48×10^{-3}	1.58×10^{-3}	7.72×10^{-1}	1.96			4.65×10^{5}	5.98×10^{2}	
4	1.38×10^{-3}	$.63\times10^{-3}$	5.67×10^{-1}	1.44			1.85×10^{5}	2.38×10^{2}	
5	5.51×10^{-4}	2.50×10^{-4}	4.17×10^{-1}	1.06			7.38×10^{4}	9.48x10	2.70×10^{-5}
6	2.19×10^{-4}	$.99\times10^{-4}$	3.07×10^{-1}	7.80×10^{-1}			2.94×10^{4}	3.77x10	$.84\times10^{-4}$
7	8.73×10^{-5}	3.96×10^{-5}	2.26×10^{-1}	5.74×10^{-1}			1.16×10^{4}	1.50x10	2.68×10^{-4}
8	3.48×10^{-5}	1.58×10^{-5}	1.66×10^{-1}	4.22×10^{-1}	88,560	27	4.33×10^{3}	5.56	6.72×10^{-4}
9	1.38×10^{-5}	$.63\times10^{-5}$	1.22×10^{-1}	3.10×10^{-1}	85,280	26	1.60×10^{3}	2.06	1.70×10^{-3}
10	5.51×10^{-6}	2.50×10^{-6}	9.02×10^{-2}	2.29×10^{-1}	82,000	25	5.88×10^{2}	7.55×10^{-1}	4.24×10^{-3}
11	2.19×10^{-6}	$.99\times10^{-6}$	6.61×10^{-2}	1.68×10^{-1}	78,720	24	2.16×10^{2}	2.78×10^{-1}	$.84\times10^{-2}$
12	8.73×10^{-7}	3.96×10^{-7}	4.88×10^{-2}	1.24×10^{-1}	75,440	23	7.89x10	1.01×10^{-1}	2.68×10^{-2}
13	3.48×10^{-7}	1.58×10^{-7}	3.58×10^{-2}	9.09×10^{-2}	72,160	22	2.87x10	3.69×10^{-2}	6.72×10^{-2}
14	1.38×10^{-7}	$.63\times10^{-7}$	2.63×10^{-2}	6.68×10^{-2}	68,880	21	1.04x10	1.34×10^{-2}	1.70×10^{-1}
15	5.51×10^{-8}	2.50×10^{-8}	1.94×10^{-2}	4.93×10^{-2}	65,600	20	3.76	4.83×10^{-3}	4.24×10^{-1}
16	2.19×10^{-8}	$.99\times10^{-8}$	1.43×10^{-2}	3.63×10^{-2}	62,320	19	1.35	1.73×10^{-3}	.84
17	8.73×10^{-9}	3.96×10^{-9}	1.05×10^{-2}	2.67×10^{-2}	59,040	18	4.83×10^{-1}	6.21×10^{-4}	2.68
18	3.48×10^{-9}	1.58×10^{-9}	7.72×10^{-3}	1.96×10^{-2}	55,760	17	1.72×10^{-1}	2.21×10^{-4}	6.72
19	1.38×10^{-9}	$.63\times10^{-9}$	5.67×10^{-3}	1.44×10^{-2}	52,480	16	6.05×10^{-2}	7.77×10^{-5}	1.70x10
20	5.51×10^{-10}	2.50×10^{-10}	4.17×10^{-3}	1.06×10^{-2}	49,200	15	2.12×10^{-2}	2.72×10^{-5}	4.24x10

TABLE II. - WEIGHT OF INTERSTAGE SECTION

[Stainless steel.]

Vehicle	Weight, lb (kg)	
	Pressure-stabilized	Stringers and skin
1	530 (240)	1100 (499)
2	460 (209)	1000 (454)
3	800 (363)	2600 (1179)

TABLE IV. - NUCLEAR-SHIELD CALCULATION RESULTS

Vehicle	1	2	3
Allowable dose, rads	10^9	10^9	10^9
Q_{req}, Btu/sec	240.7	121.0	324.0
D/P_R, rads/(hr)(mw)	0.0038×10^9	0.001×10^9	0.001×10^9
t_{LiH}, in.	0	4	4
t_{Fe}, in.	0	0	0
$Q/A_{sh}P_R$, Btu/(sec)(cm^2)(mw)	2.7×10^{-4}	0.88×10^{-4}	0.88×10^{-4}
P_R, mw	25	150	400
Q/A, Btu/(sec)(cm^2)	67.5×10^{-4}	132×10^{-4}	352×10^{-4}
A, cm^2	8180	8640	8640
Q, Btu/sec	55.2	114	304
D, rads/hr	0.095×10^9	0.15×10^9	0.4×10^9
Time on, hr	3.462	0.404	0.367
Dose, rads	0.329×10^9	0.061×10^9	0.147×10^9
Weight, lb (kg)	0	150 (68)	150 (68)

TABLE V. - FLIGHT CONDITIONS IN EARTH'S ATMOSPHERE

Time, sec	Altitude		Velocity[a]		Mach number
	ft	km	ft/sec	m/sec	
0	0	0	1350	411	0.0
20	3,141	.957	1414	431	.3
40	13,566	4.135	1710	521	.7
60	32,307	9.847	2291	698	1.3
80	59,862	18.246	3178	969	2.2
100	97,037	29.577	4439	1353	3.3
120	144,778	44.128	6117	1864	4.5
140	204,987	62.480	8286	2526	6.9
145	221,255	67.439	8923	2720	7.7

[a]Absolute velocity with respect to Earth's center.

TABLE VI. - HEAT INPUT TO HYDROGEN DURING FIRST POWER-ON PHASE (BTU/SEC)

[Must add additional heat to hydrogen by line from reactor.
For vehicles 2 and 3, very little heat must be added.]

Source	Vehicle		
	1	2	3
Nuclear heating	55.2	114.0	304.0
Thermal heating:			
Thermal radiation from control compartment	Negligible		
Thermal radiation from payload	Negligible		
Conduction through struts from payload	Negligible		
Conduction through conical structure	Negligible		
Sun-Earth radiation:			
Sun to tank	3.3	2.7	5.2
Earth to tank	.7	1.6	2.8
Four vertical sides of tank	.3	1.4	2.9
Total heating obtained	59.5	119.7	314.9
Heating required for reactor cooling and maintaining constant tank pressure	240.7	121.0	324.0

TABLE VII. - HEAT INPUT TO HYDROGEN DURING SECOND POWER-ON PHASE (BTU/SEC)

[Must add additional heat to hydrogen by line from reactor.
For vehicles 2 and 3, very little heat must be added.]

Source	Vehicle		
	1	2	3
Nuclear heating	55.2	114.0	304.0
Thermal heating:			
Thermal radiation from control compartment	Negligible		
Thermal radiation from payload	Negligible		
Conduction through struts from payload	Negligible		
Conduction through conical structure	Negligible		
Sun-Mars radiation:			
Sun to tank	2.1	1.7	3.3
Mars to tank	.4	.3	.7
Four vertical sides of tank	.2	.2	.3
Total heating obtained	57.9	116.2	308.3
Heating required for reactor cooling and maintaining constant tank pressure	240.7	121.0	324.0

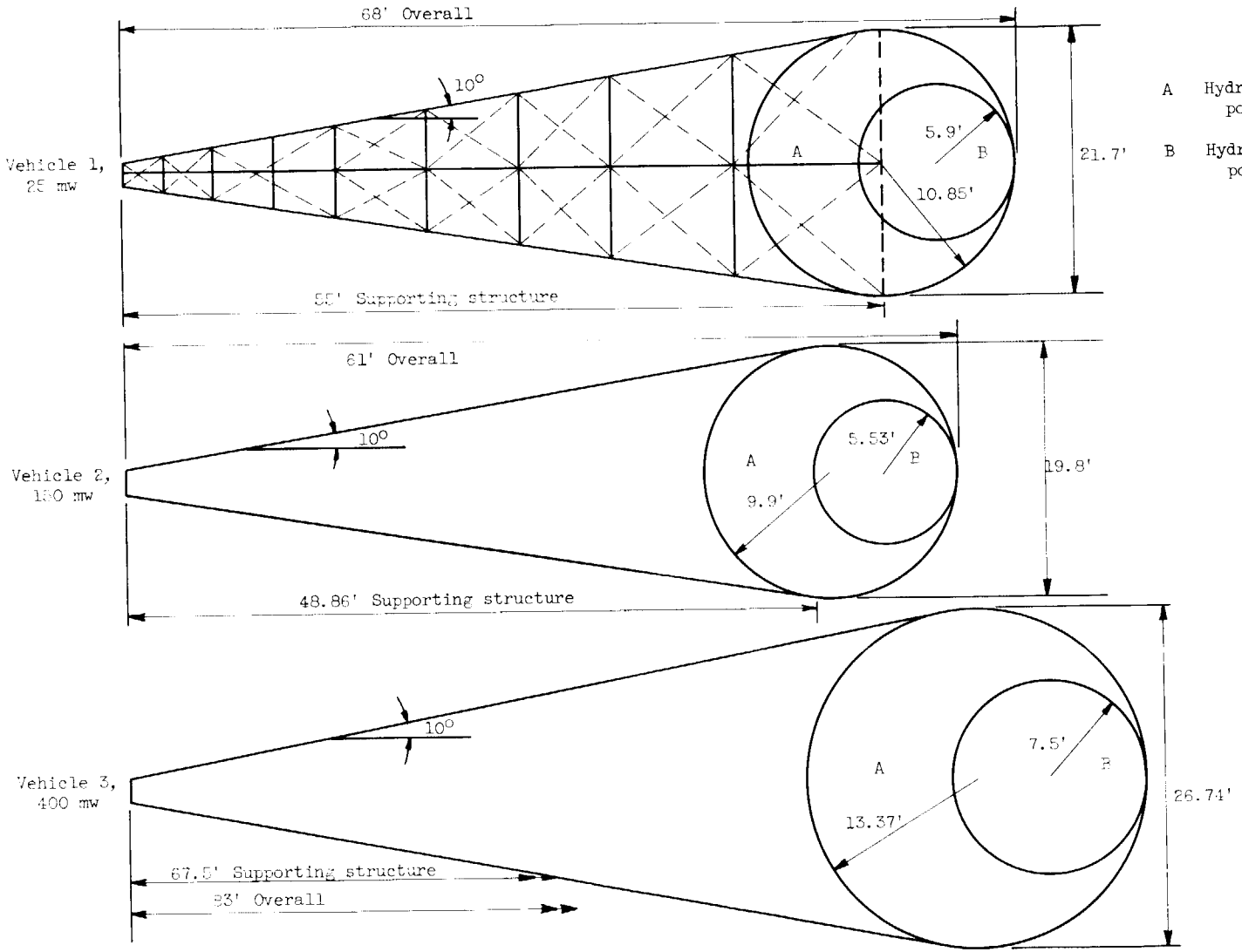

Figure 1. - Double-spherical-tank concept.

TABLE VIII. - HEAT INPUT TO HYDROGEN AT END OF COAST PHASE (BTU/SEC)

Source	Vehicle		
	1	2	3
Nuclear heating	0.0000122	0.0000066	0.000014
Thermal heating:			
Thermal radiation from control compartment	.00208	.00212	.00212
Thermal radiation from payload	.000824	.000824	.000824
Conduction through struts from payload	.000335	.000335	.000335
Conduction through conical structure	.001644	.001549	.001549
Solar radiation	None	None	None
Total heating obtained	0.0048952	0.0048346	0.004842
Heating required for reactor cooling and maintaining constant tank pressure	0.000086	0.000047	0.0001

TABLE IX. - MICROSCOPIC REMOVAL CROSS SECTIONS

[Taken from ref. 15.]

Material	$\sigma_{r,i}$ barns
Tungsten	2.51
Uranium	3.6
Oxygen	.99
Beryllium	1.07
Hydrogen	1.00
Lithium	1.01
Iron	1.98

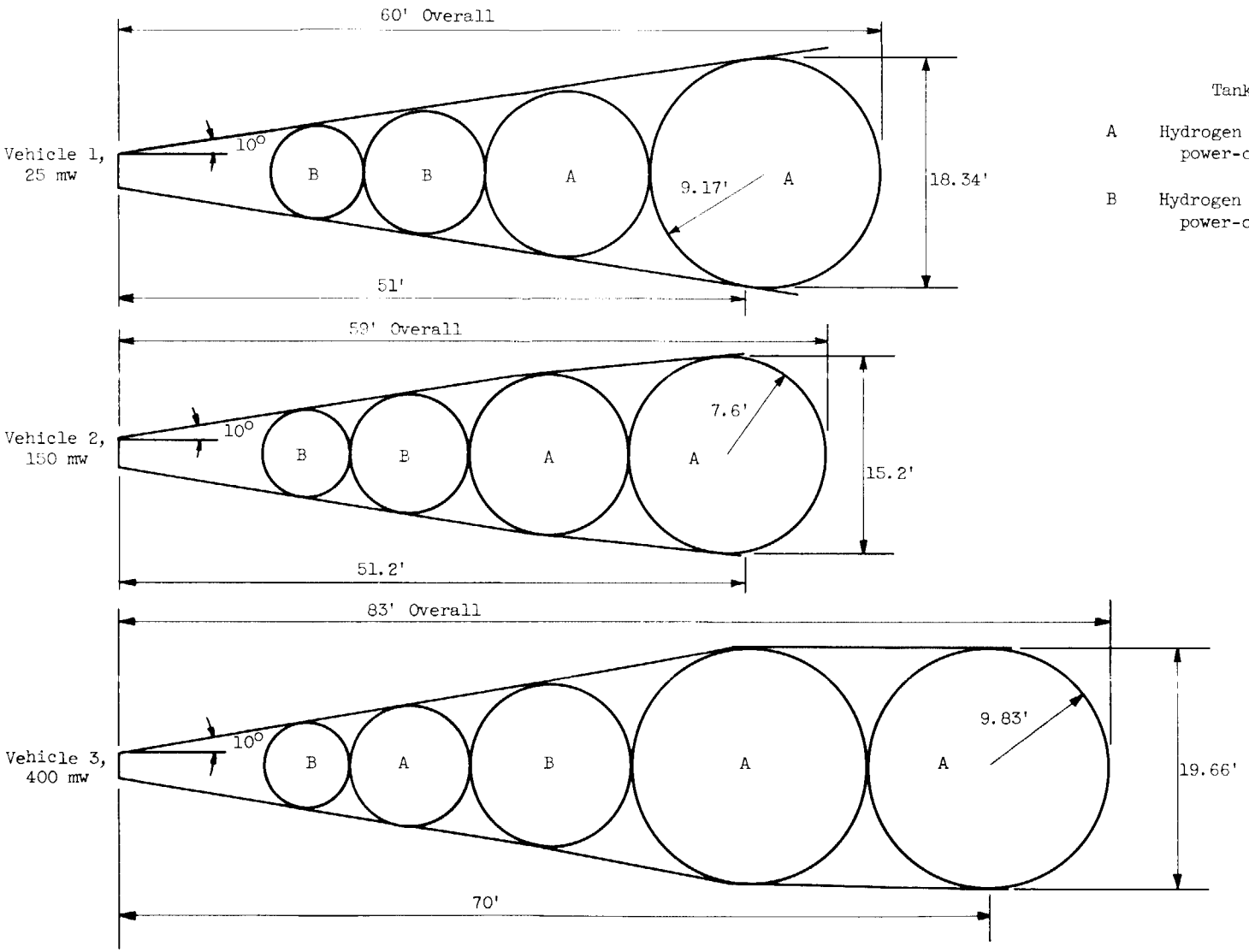

Figure 2. - Multiple-spherical-tank concept. (Note: Outer skin between spheres in all vehicles pressurized.)

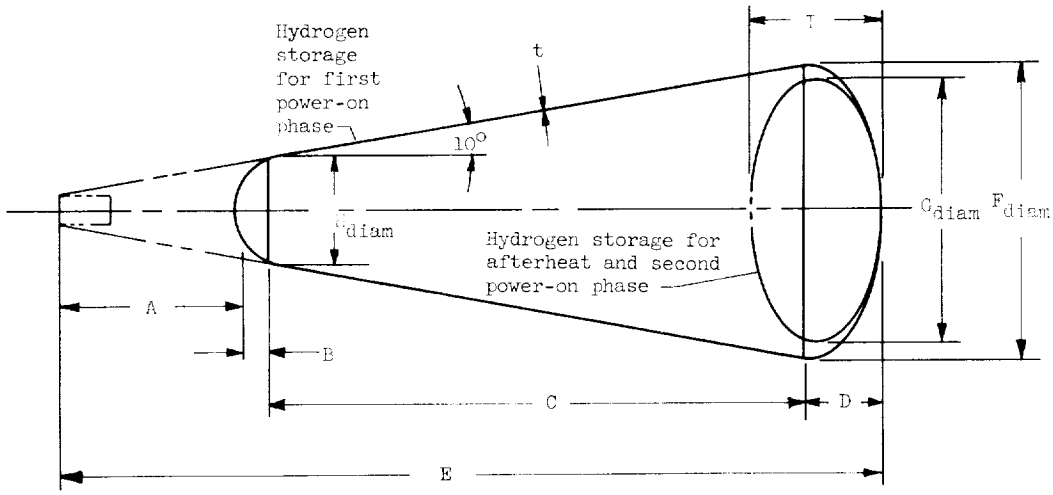

Vehicle tank dimensions

Vehicle[a]	Power, mw	A	B	C	D	E	F	G	H	I
1	25	11' 0"	1' $7\frac{1}{4}$"	34' 2"	4' $7\frac{1}{8}$"	51' $4\frac{3}{8}$"	18' $4\frac{5}{8}$"	14' $11\frac{5}{8}$"	3' $2\frac{1}{2}$"	7' $5\frac{7}{8}$"
2	150	11' 8"	1' 9"	29' 2"	4' $2\frac{1}{2}$"	46' $8\frac{1}{2}$"	16' 10"	13' $11\frac{1}{2}$"	3' 4"	6' $11\frac{3}{4}$"
3	400	11' 8"	1' 8"	46' 3"	5' $8\frac{5}{8}$"	65' $3\frac{5}{8}$"	22' $10\frac{5}{8}$"	18' $10\frac{1}{2}$"	3' 4"	9' $5\frac{1}{4}$"

[a]Material, 2014-T6 aluminum.

Vehicle tank statistics

Vehicle	Power, mw	Tank weight, lb		Tank volume, cu ft		Wall thickness, t, in.		Tank pressure, lb/sq in. abs
		Inner	Outer	Inner	Outer	Inner	Outer	Inner and outer
1	25	1375	2025	880	5325	0.11	0.034-0.093	50
2	150	1200	1508	710	4045	0.10	0.034-0.085	50
3	400	3100	4038	1764	9983	0.14	0.034-0.116	50

Figure 3. - Cone-tank concept.

E-974

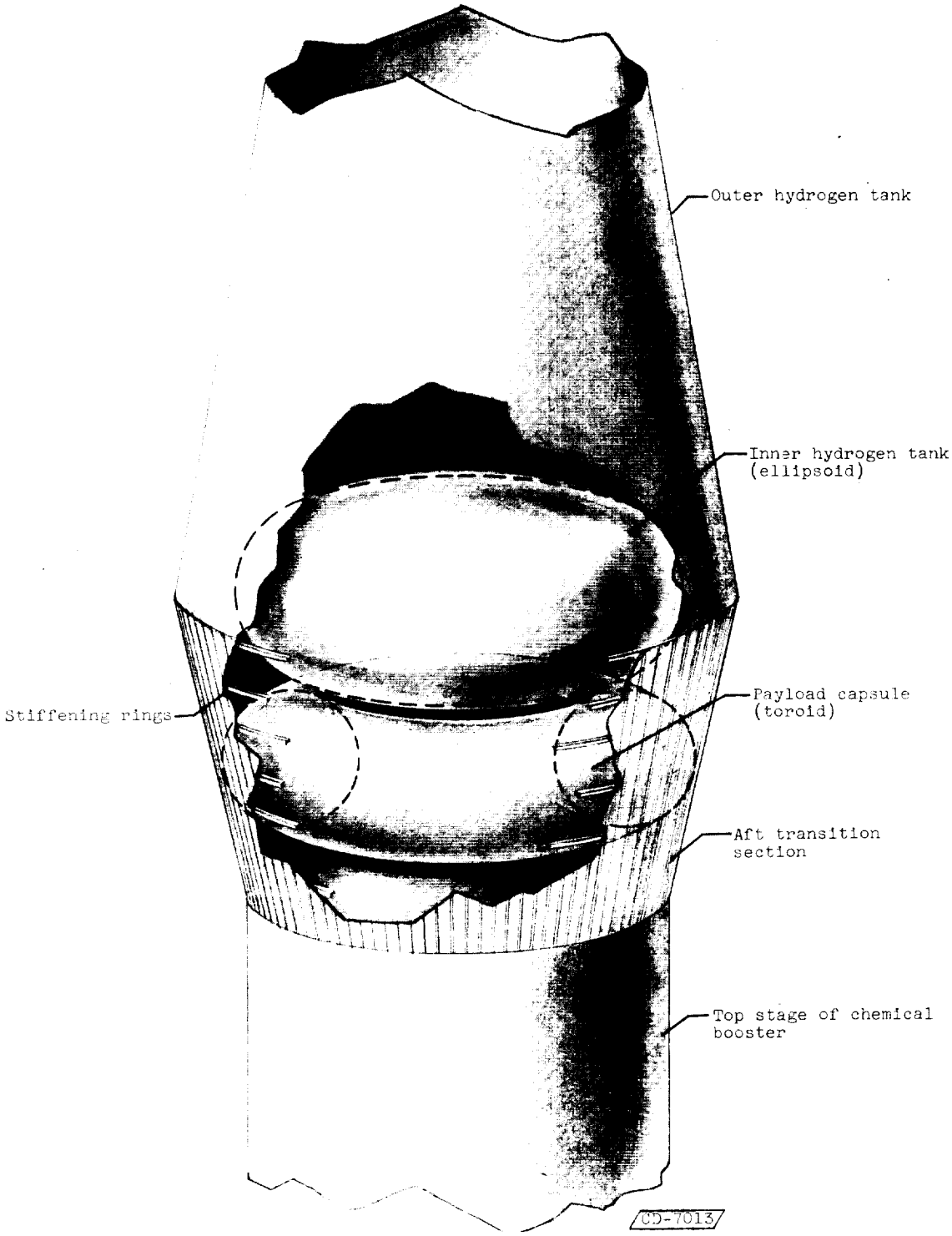

Figure 4. - Detail of structure between top chemical stage and nuclear stage.

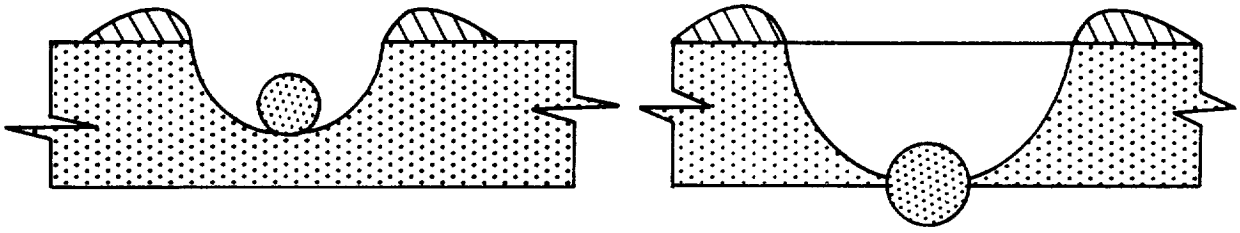

(a) Nonpenetrating meteoroid. (b) Penetrating meteoroid.

Figure 5. - Assumed meteoroid crater shapes in tank walls.

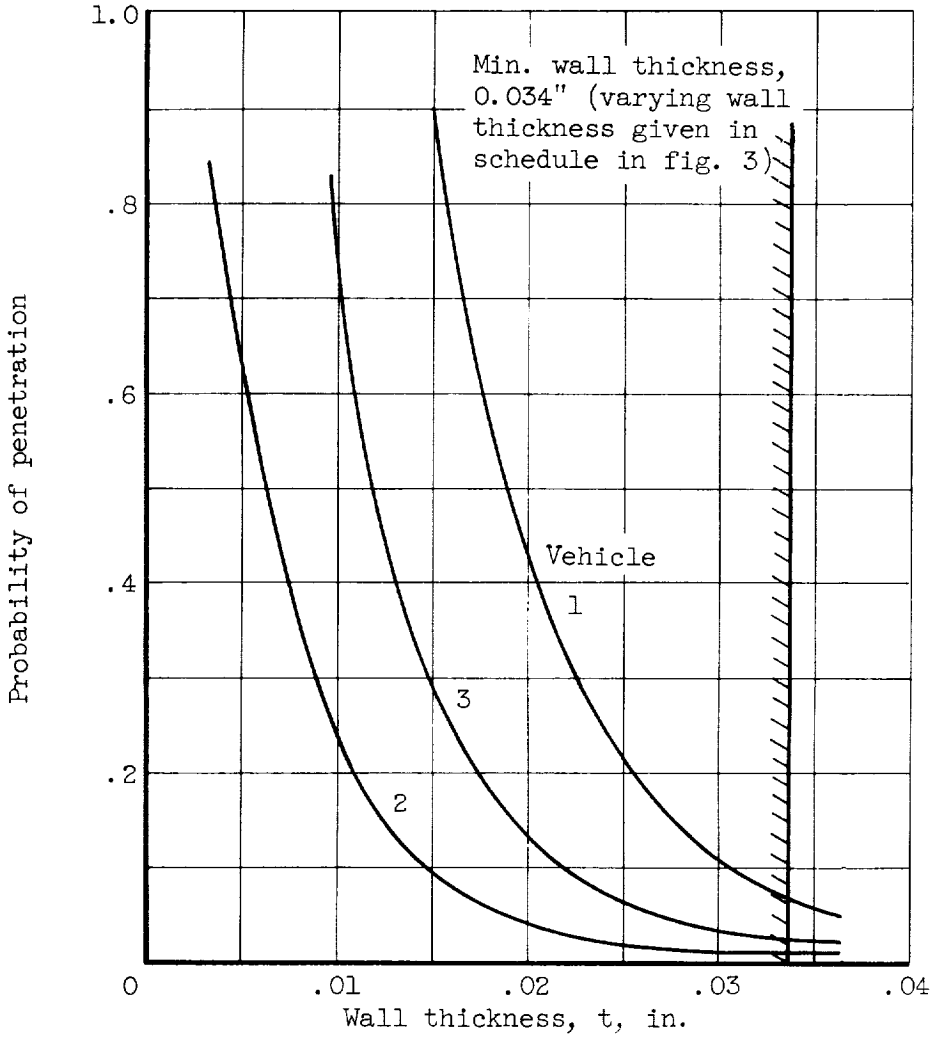

Figure 6. - Probability of meteoroid penetration of outer aluminum conical tank during spiraling period as function of wall thickness.

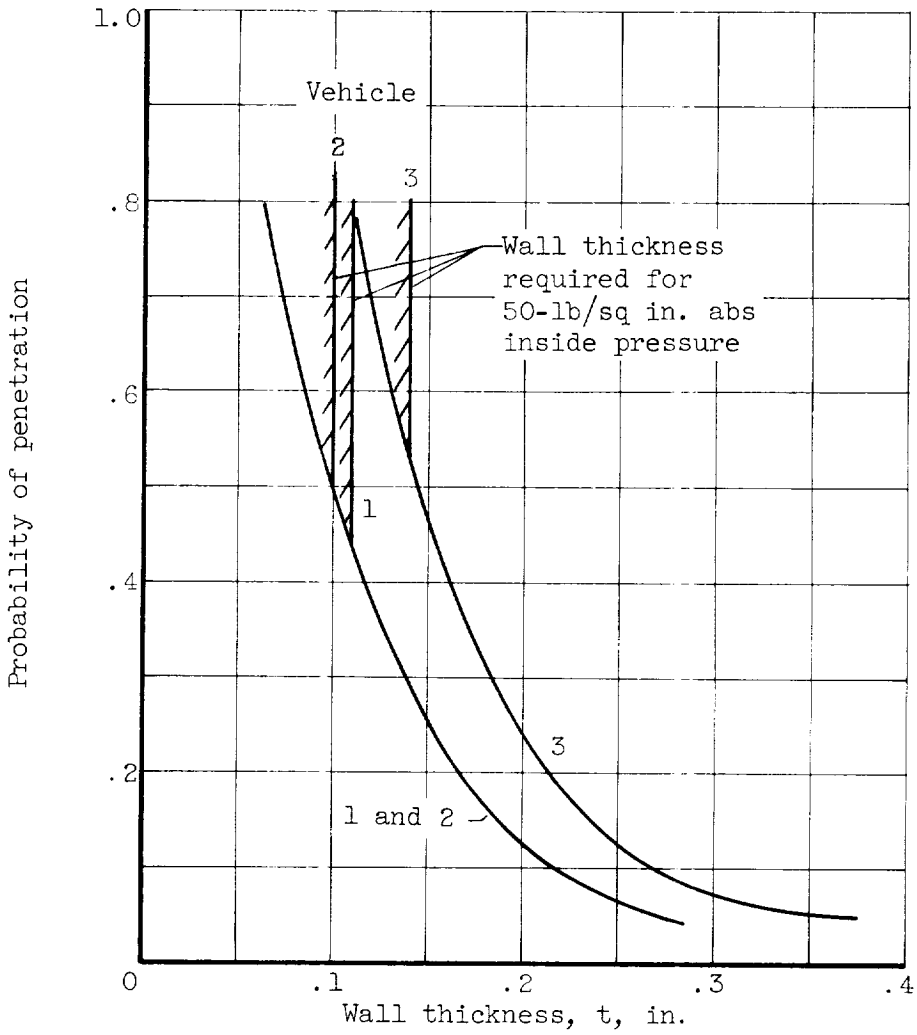

Figure 7. - Probability of meteoroid penetration of inner aluminum tank during coasting period as function of wall thickness.

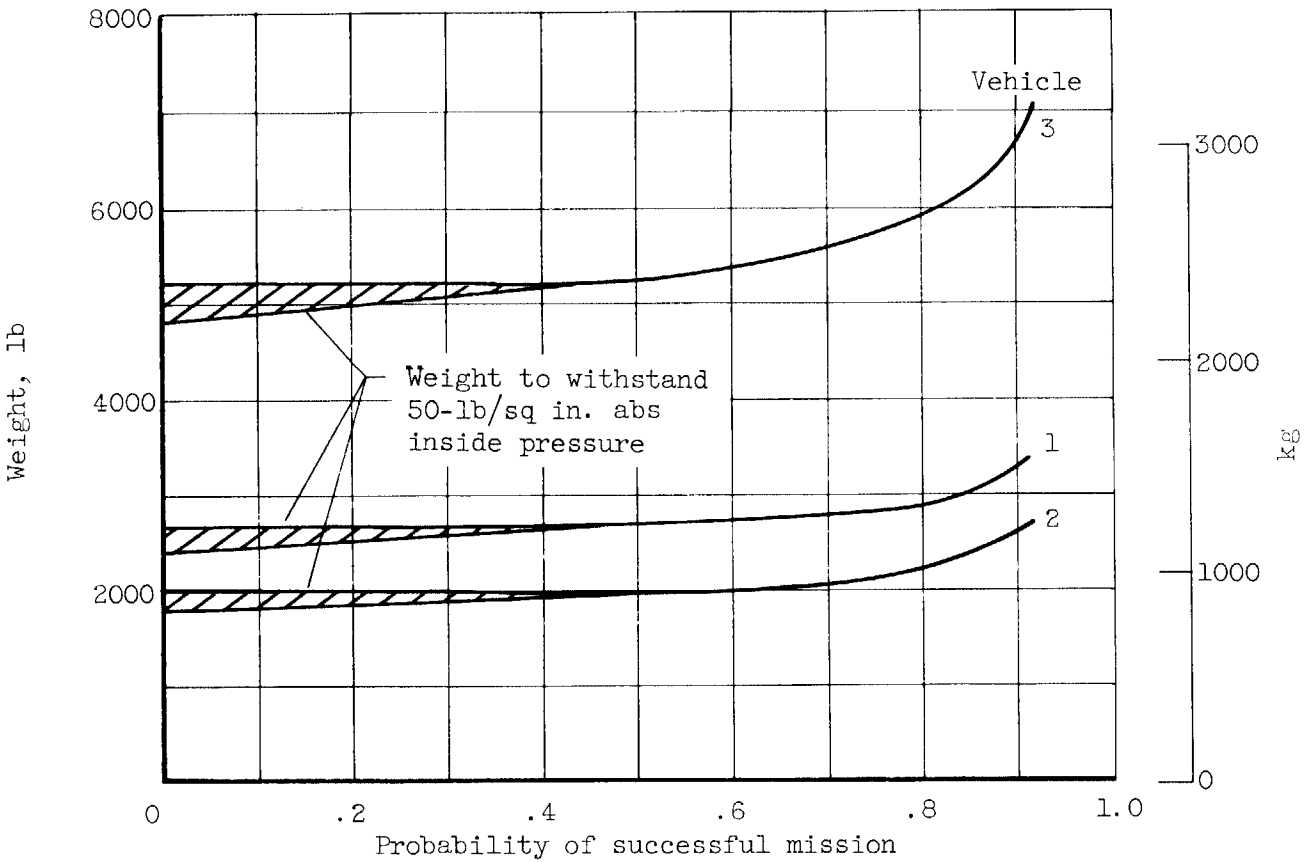

Figure 8. - Combined weight of inner and outer tanks as function of probability of success during complete mission.

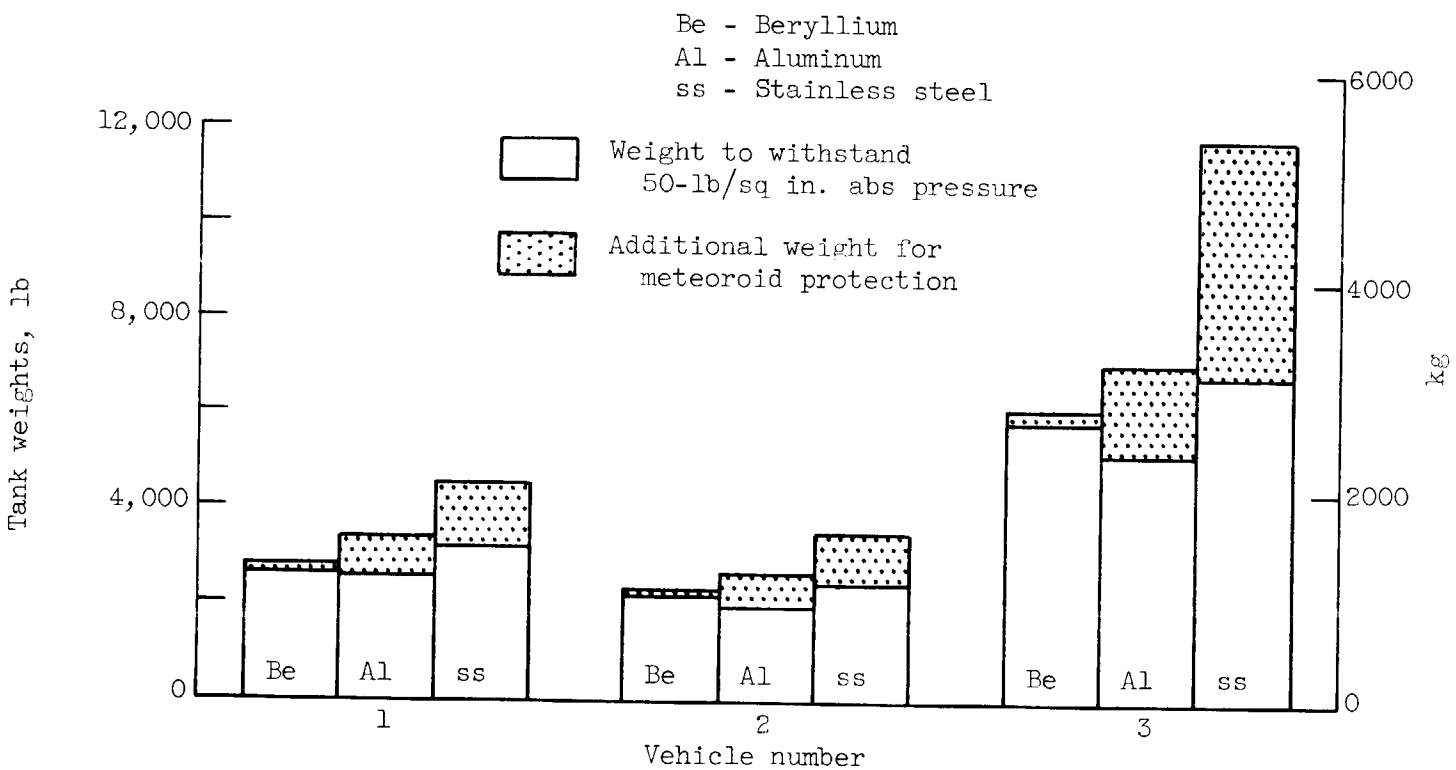

Figure 9. - Comparison of weights of beryllium, aluminum. and stainless steel as materials for tanks.

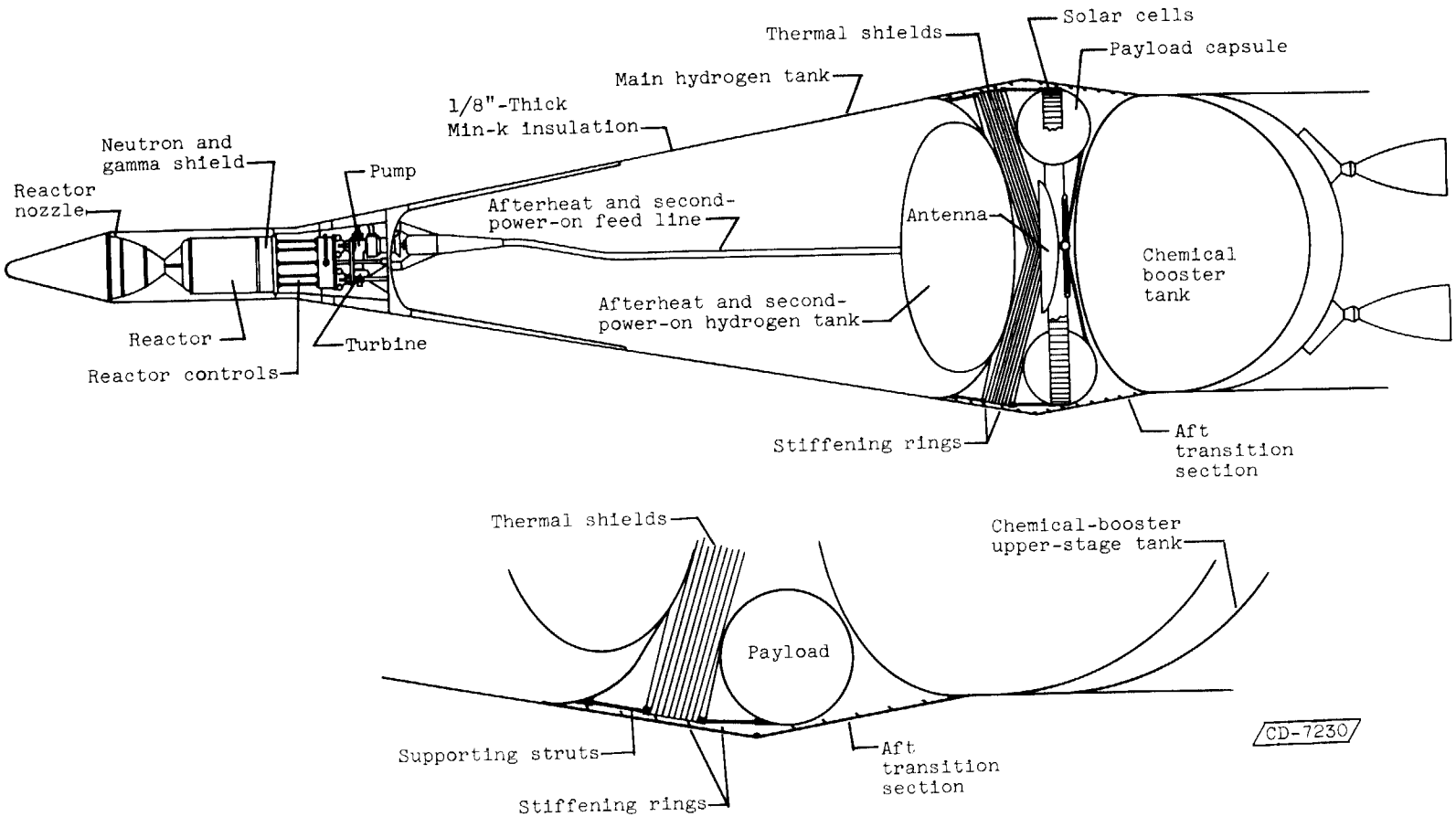

Detail of aft transition section and insulating struts

Figure 10. - Details of tanks insulating components.

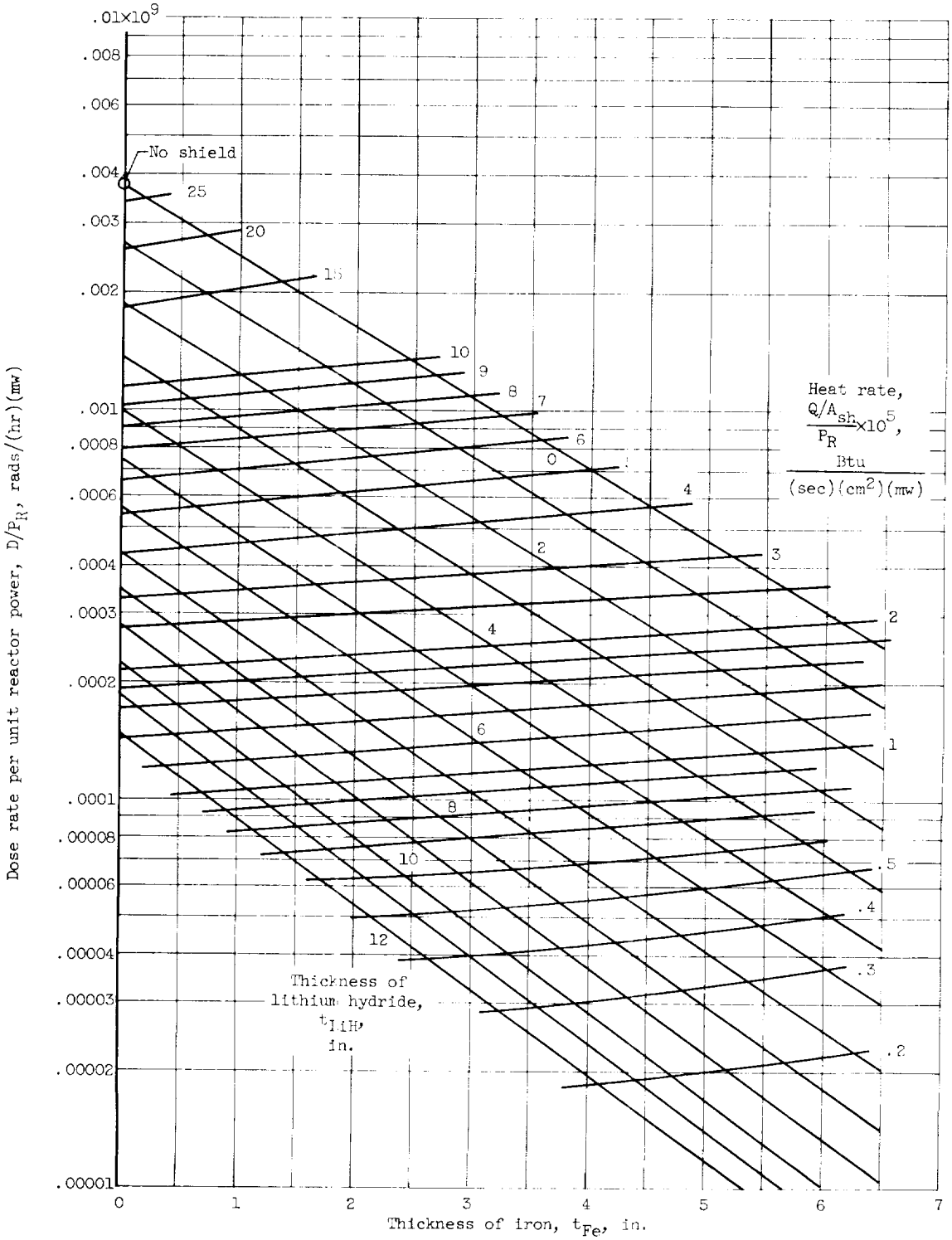

Figure 11. - Correlation of dose, heat rate, and nuclear-shield thickness.

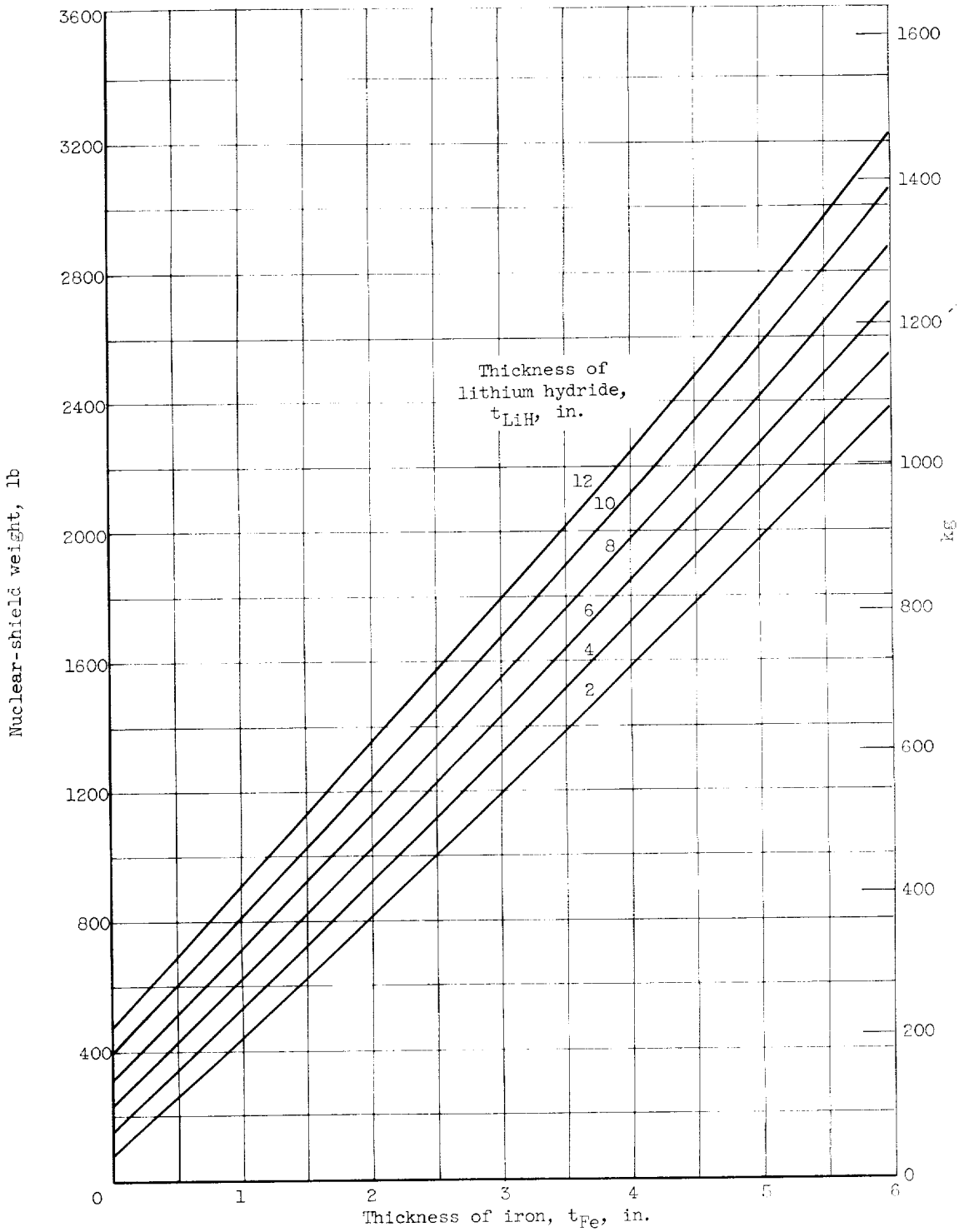

Figure 12. - Weight of nuclear shields made from lithium hydride and iron.

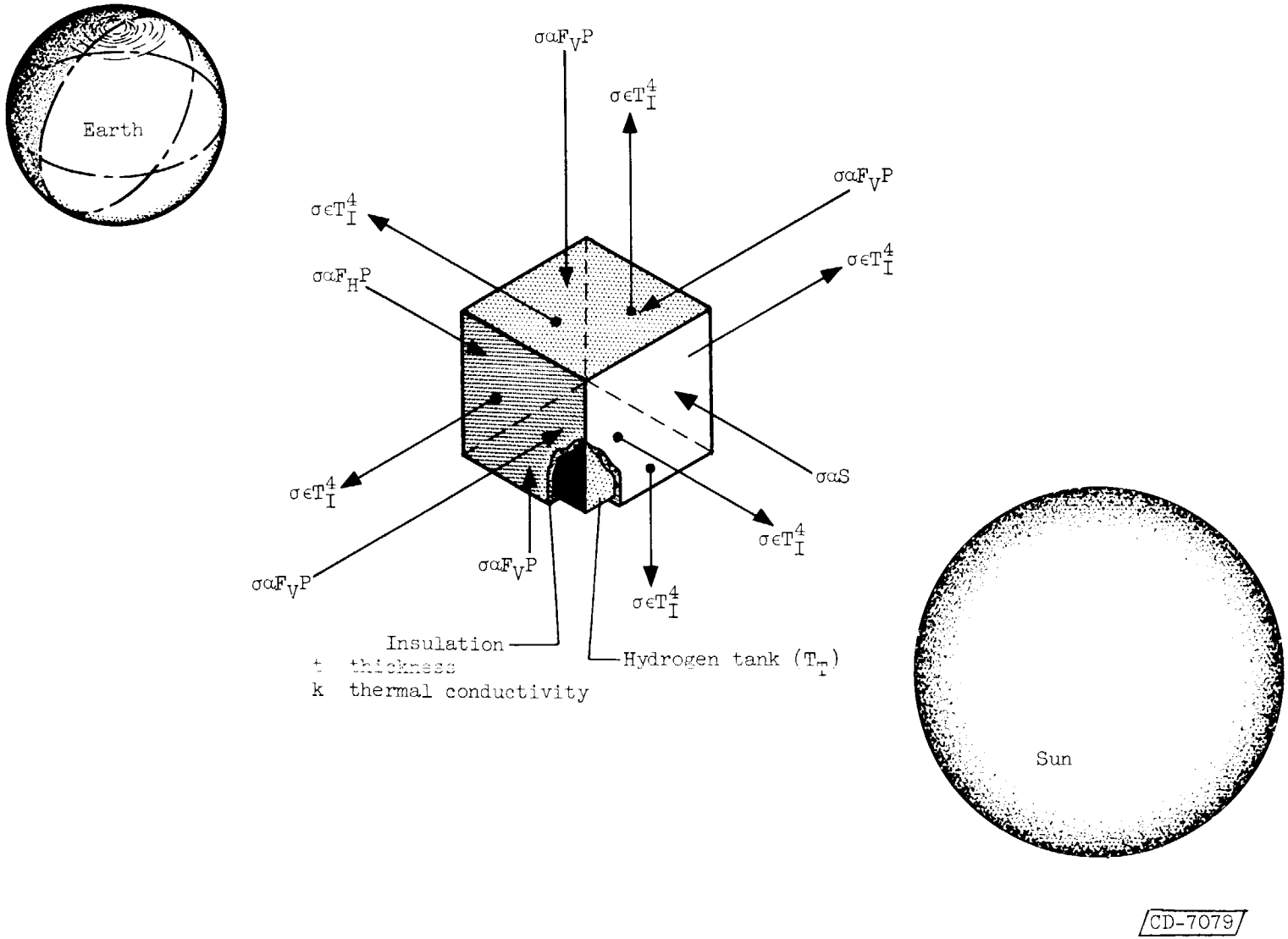

Figure 13. - Sun-Earth radiation heat inputs to hydrogen tank.

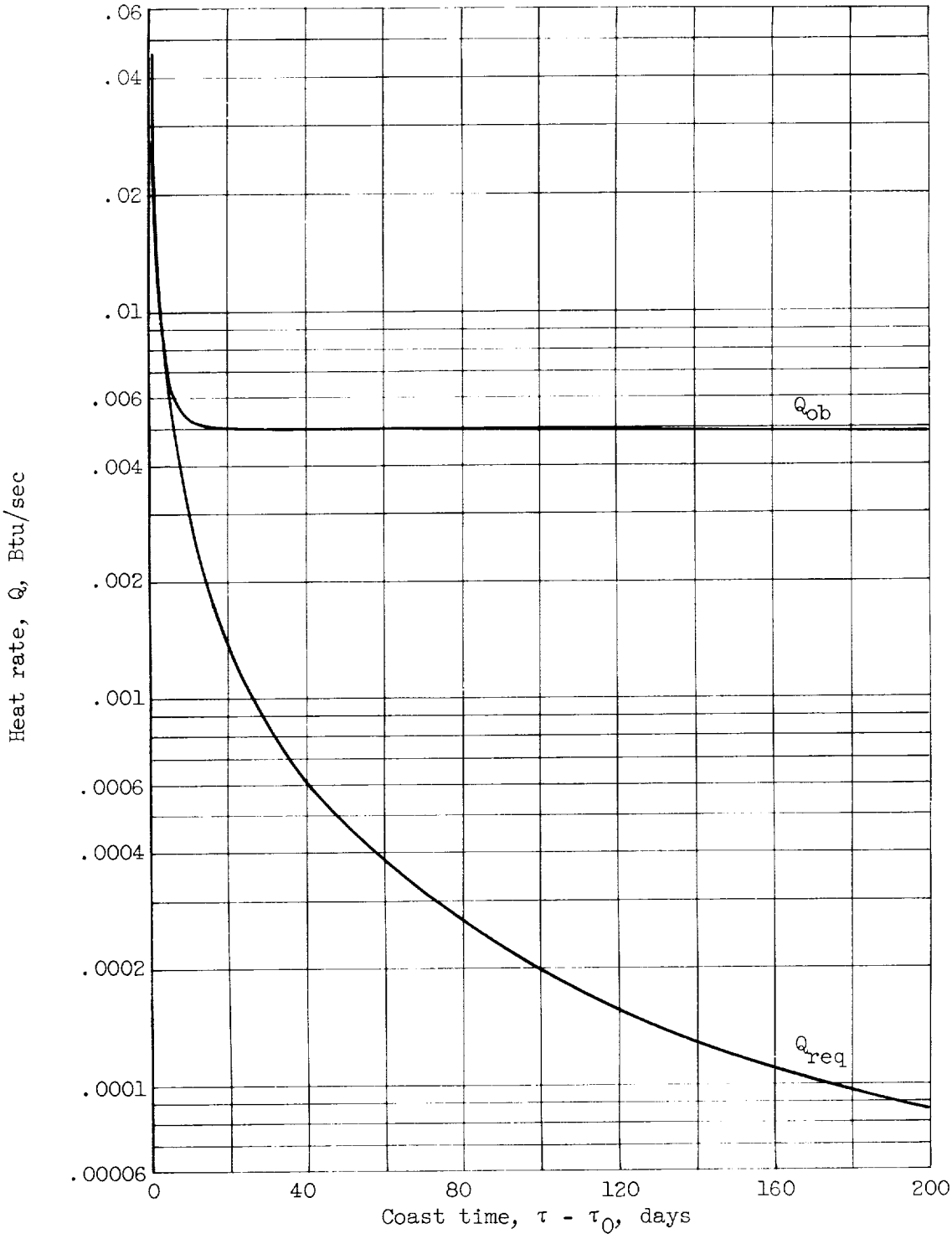

(a) Vehicle 1; reactor power, 25 megawatts.

Figure 14. - Heat input to hydrogen during coast.

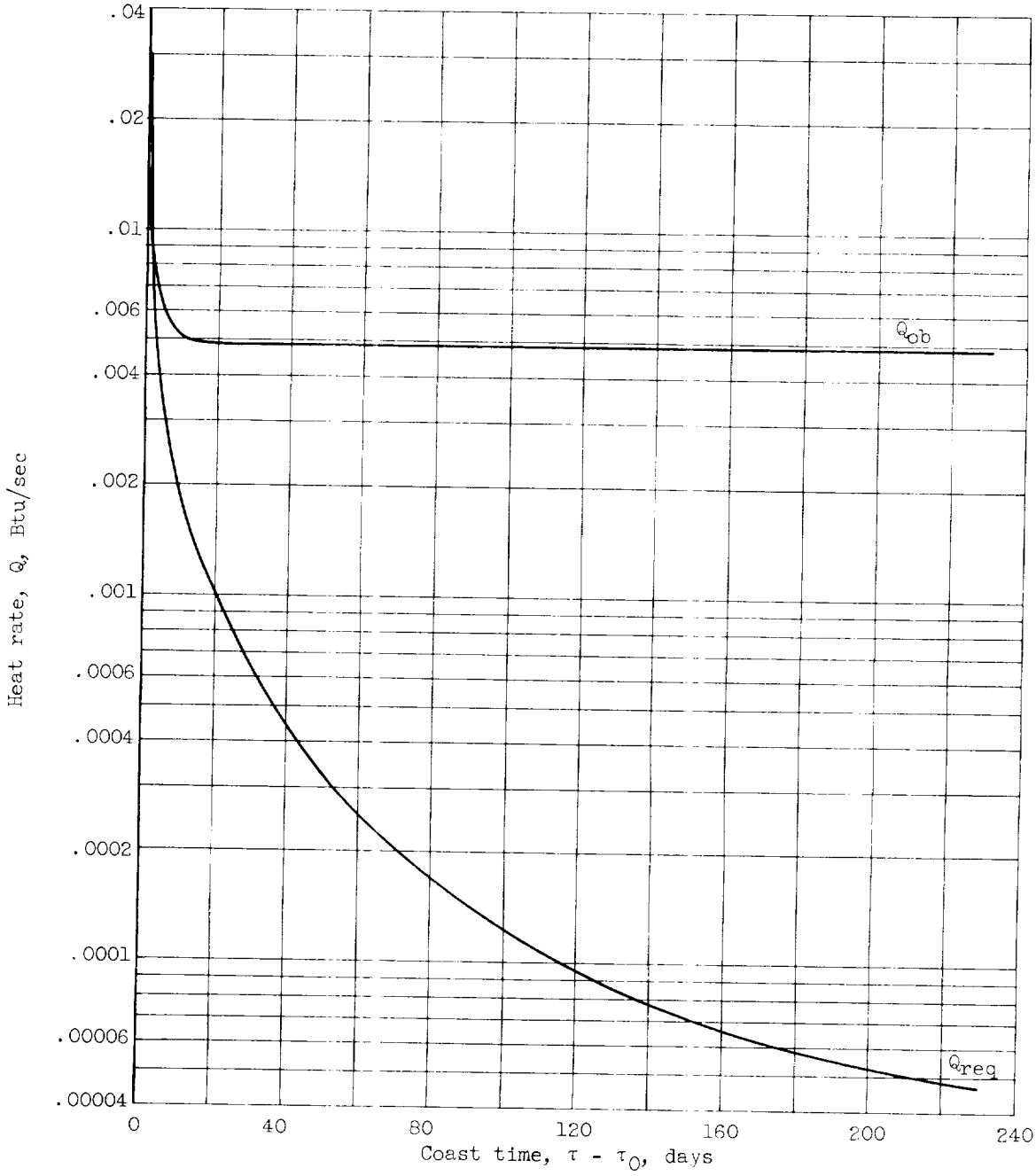

(b) Vehicle 2; reactor power, 150 megawatts.

Figure 14. - Continued. Heat input to hydrogen during coast.

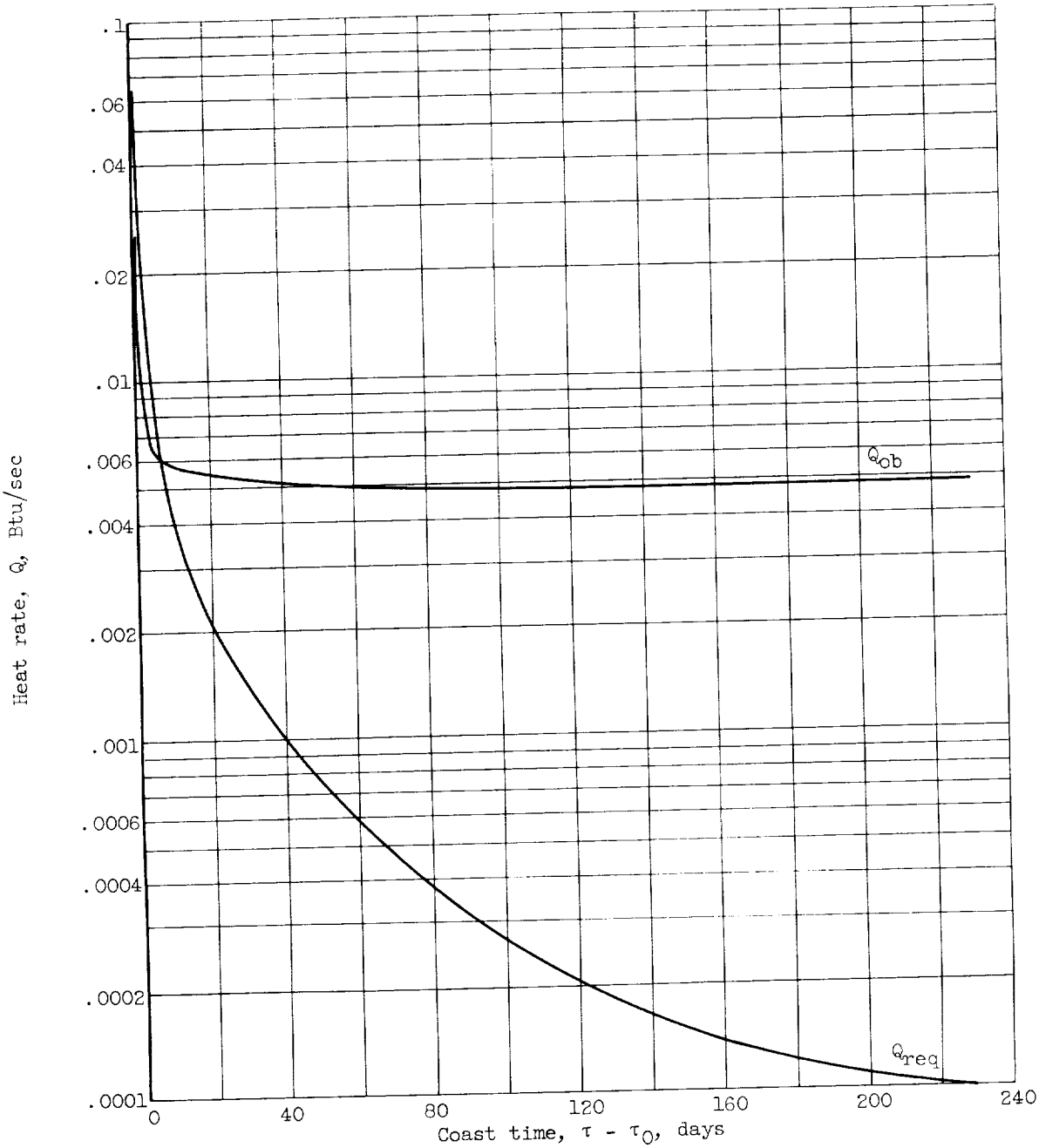

(c) Vehicle 3; reactor power, 400 megawatts.

Figure 14. - Concluded. Heat input to hydrogen during coast.

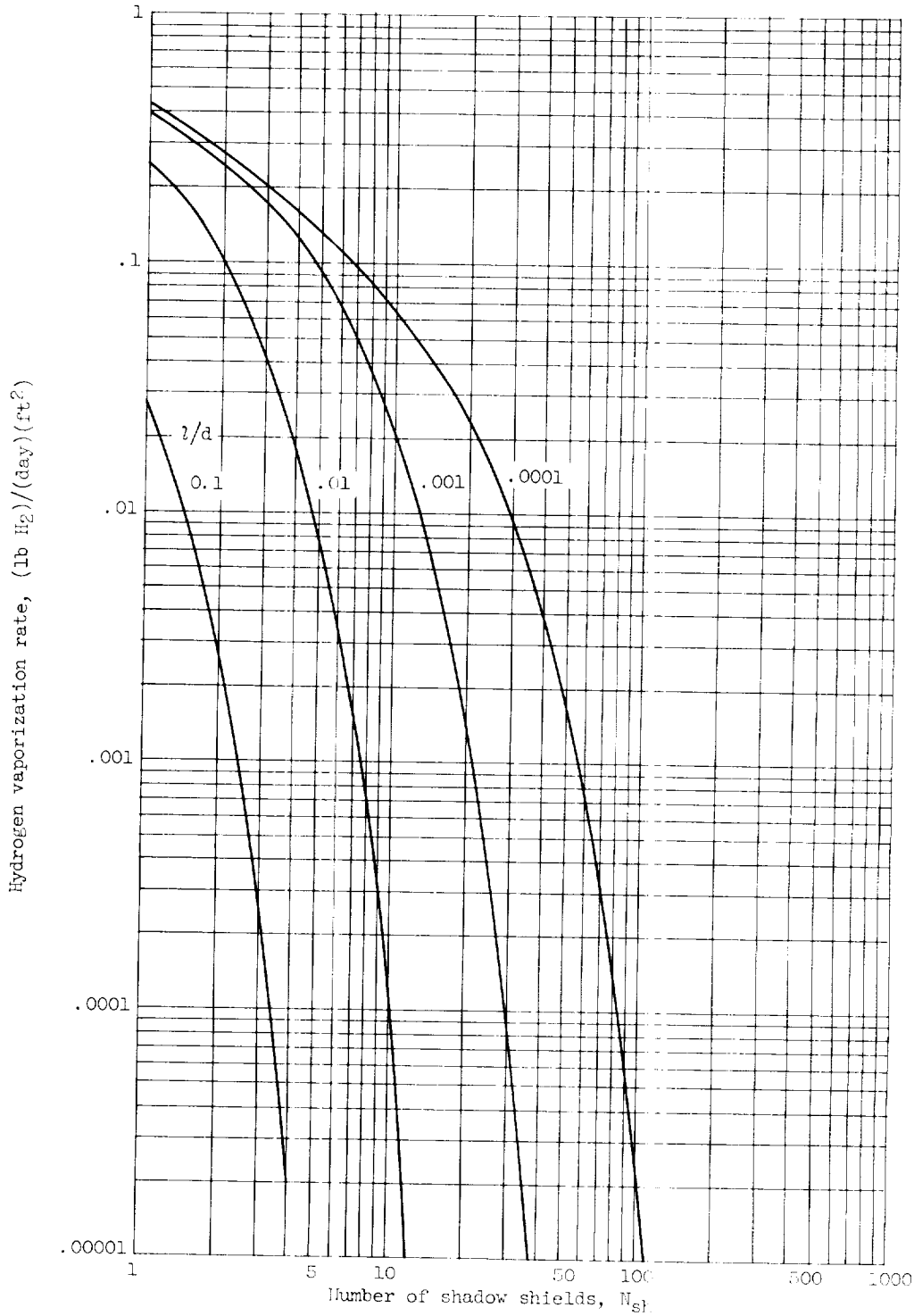

Figure 15. - Hydrogen vaporization rate from payload at 520° R through shadow shields at various spacings from hydrogen tank. Absorptivity, 0.1; emissivity, 0.1; latent heat of vaporization, 194.27 Btu per pound.

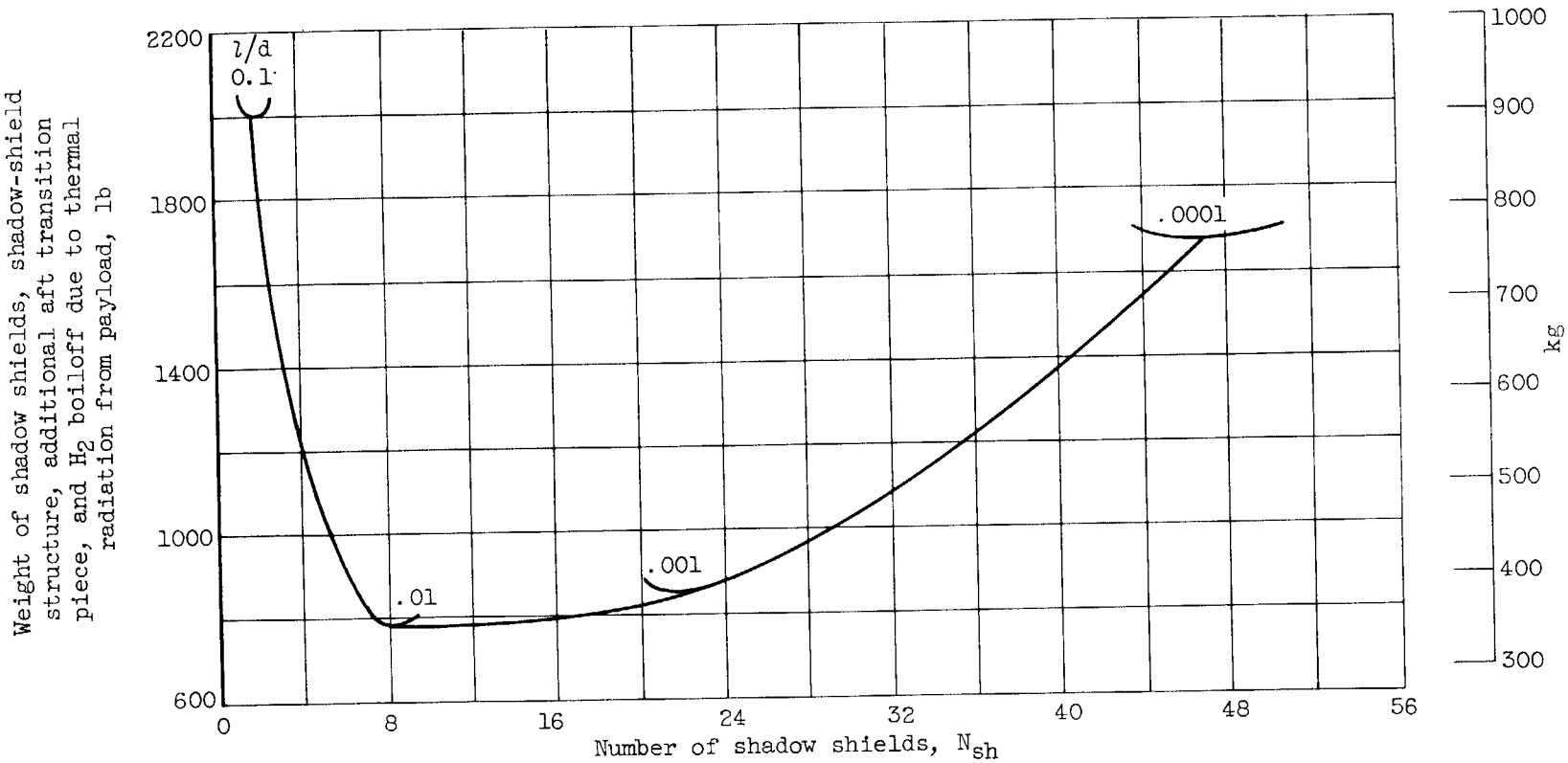

Figure 16. - Determination of number and spacing of shadow shields between payload and tank during coast phase for vehicle 3.

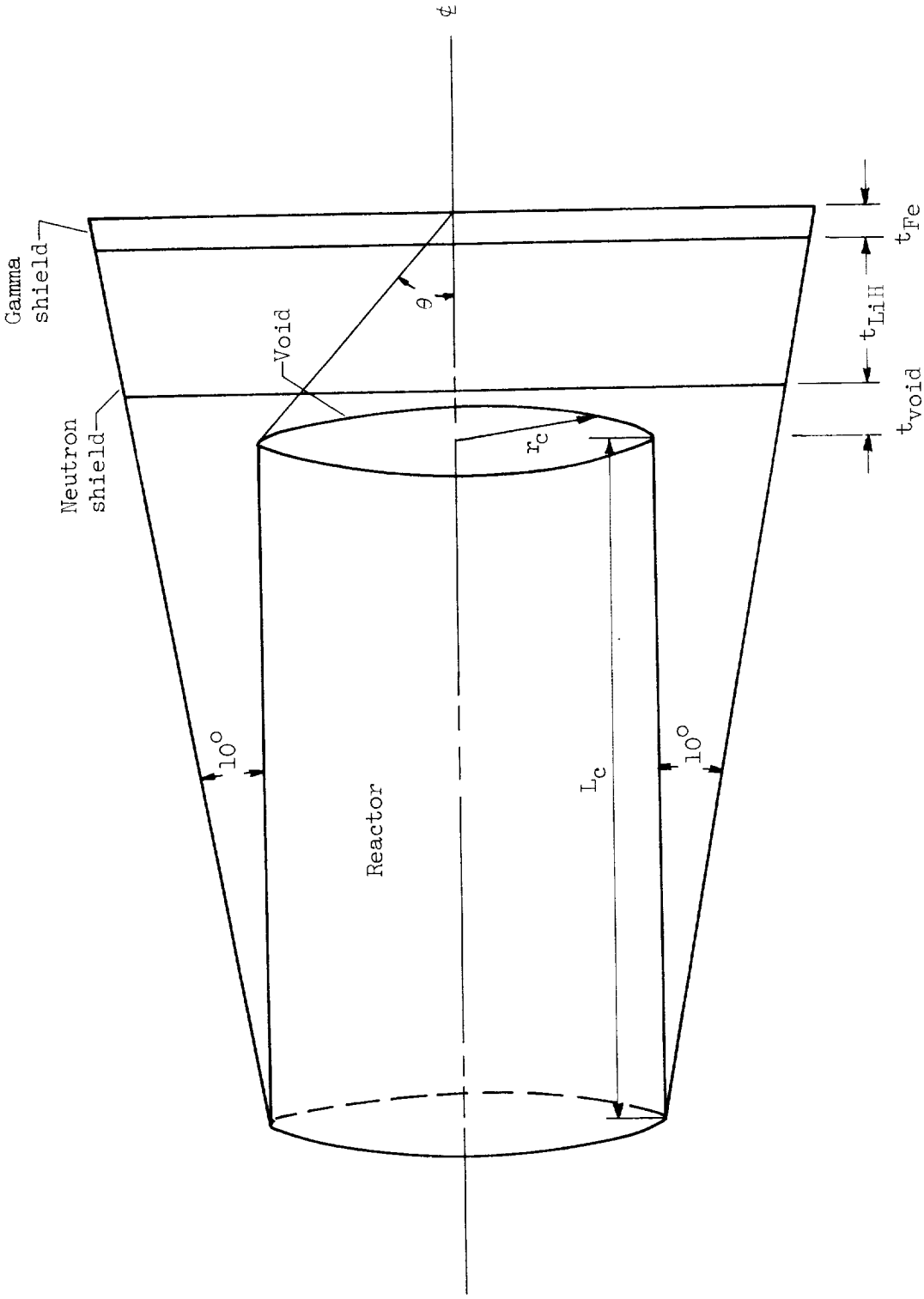

Figure 17. - Schematic sketch showing location of nuclear shield.